Neuropeptide Y expression defines a novel class of GABAergic projection neurons in the inferior colliculus

Abbreviated title: NPY neurons and NPY signaling in the IC

Marina A. Silveira[1], Justin D. Anair[1], Nichole L. Beebe[2], Brett R. Schofield[2], Michael T. Roberts[1,]*

1. Kresge Hearing Research Institute, Department of Otolaryngology – Head and Neck Surgery, University of Michigan, Ann Arbor, Michigan 48109

2. Department of Anatomy and Neurobiology, Northeast Ohio Medical University, Rootstown, Ohio 44272

*Corresponding author: microb@umich.edu

Abstract

Located in the midbrain, the inferior colliculus (IC) integrates information from numerous auditory nuclei and is an important hub for sound processing. Despite its importance, little is known about the molecular identity and functional roles of defined neuron types in the IC. Using a multifaceted approach in mice, we found that neuropeptide Y (NPY) expression identifies a major class of inhibitory neurons, accounting for approximately one-third of GABAergic neurons in the IC. Viral tract tracing showed that NPY neurons are principal neurons, with axons that project locally and to the auditory thalamus and contralateral IC. In brain slice recordings, many NPY neurons fired spontaneously, suggesting an intrinsic pacemaker ability that may drive tonic inhibition onto postsynaptic targets. Morphological reconstructions showed that NPY neurons are stellate cells, and the dendrites of NPY neurons in the tonotopically-organized central nucleus of the IC cross isofrequency laminae. Immunostaining confirmed that NPY neurons express NPY, and we therefore hypothesized that NPY signaling regulates activity in the IC. In crosses between Npy1r^{cre} and Ai14 Cre-reporter mice, we found that NPY Y_1 receptor (Y_1R)-expressing neurons were broadly distributed throughout the rostro-caudal extent of the IC. In whole-cell recordings from Y_1R-expressing IC neurons, application of

a high affinity Y_1R agonist led to hyperpolarization of a subset of neurons. Thus, NPY neurons represent a novel class of inhibitory principal neurons that are well poised to use GABAergic and NPY signaling to regulate the excitability of circuits in the IC and auditory thalamus.

Introduction

The inferior colliculus (IC) is the hub of the central auditory pathway (Adams, 1979; Cant and Benson, 2006, 2007), a critical processing center for most aspects of hearing, and an important site of plasticity after hearing loss (Chambers et al., 2016; Sturm et al., 2017). Despite its importance in auditory processing, it has proven difficult to identify the neuron classes that comprise the IC (Peruzzi et al., 2000; Palmer et al., 2013; Beebe et al., 2016). As a result, the cellular organization and function of neural circuits in the IC remain largely unclear.

The IC contains three main subdivisions: the central nucleus (ICc), dorsal cortex (ICd), and lateral cortex (IClc) (Morest and Oliver, 1984; Faye-Lund and Osen, 1985). The ICc is tonotopically organized into isofrequency laminae, and neurons in the ICc are divided in two broad morphological families: disc-shaped and stellate neurons (Meininger et al., 1986; Malmierca et al., 1993). Disc-shaped neurons, the majority of neurons, maintain their dendritic arbors within isofrequency laminae (Oliver and Morest, 1984), while stellate neurons extend their dendritic arbors across isofrequency laminae and integrate information across sound frequencies (Oliver et al., 1991). However, there is considerable diversity within the disc-shaped and stellate groups, suggesting that they contain multiple neuron types (Oliver et al., 1994; Peruzzi et al., 2000; Ono et al., 2005).

GABAergic neurons represent ~25% of neurons in the IC (Oliver et al., 1994; Merchán et al., 2005; Beebe et al., 2016). In addition to providing local inhibition, many GABAergic neurons project to the medial geniculate nucleus (MG, auditory thalamus) (Winer et al., 1996; Peruzzi et al., 1997). Anatomical studies have subdivided GABAergic neurons into classes based on soma size and extracellular markers (Ito et al., 2009; Beebe et al., 2016), and neurons in all these classes can project to the MG (Beebe et al., 2018). However, it is unclear whether these anatomically defined groups represent neuron classes with distinct functional roles.

58 In many brain regions, an approach that combines anatomical and physiological analyses
59 with molecular markers has proven key to identifying functionally distinct neuron types
60 (Tremblay et al., 2016; Zeng and Sanes, 2017). Using such an approach, we recently identified
61 vasoactive intestinal peptide (VIP) as a marker for a distinct class of excitatory principal neurons
62 in the IC (Goyer et al., 2019), but there are currently no known molecular markers for
63 GABAergic neuron classes in the IC.
64 NPY is a 36 amino-acid neuropeptide and one of the most abundant peptides in the brain
65 (Chronwall et al., 1985; O'Donohue et al., 1985). NPY is released from neurons and binds to the
66 NPY family of $G_{i/o}$-coupled G-protein coupled receptors (Dumont et al., 1998). NPY signaling
67 modulates synaptic transmission, neuronal excitability, and other physiological processes (Bacci
68 et al., 2002). Across several brain regions, NPY has proven to be an important molecular marker
69 for distinct classes of GABAergic neurons (Tong et al., 2008; Polgár et al., 2011). Because
70 previous studies suggest that NPY (Nakagawa et al., 1995) and NPY Y_1 receptors (Y_1R) are
71 expressed in the IC (Kishi et al., 2005; Eva et al., 2006), we hypothesized that NPY is a molecular
72 marker for a class of GABAergic neurons in the IC.
73 Using a multifaceted approach, we found that NPY is expressed by a distinct population of
74 GABAergic neurons in the IC. These neurons have a stellate morphology and represent
75 approximately one-third of the GABAergic neurons in the IC. Among other targets, NPY neurons
76 project to the ipsilateral and contralateral IC and the MG. In brain slice recordings, NPY neurons
77 fired spontaneously, suggesting an intrinsic pacemaker ability. Using $Npy1r^{cre}$ mice to target
78 recordings, we found that application of a Y_1R-selective agonist hyperpolarized the membrane
79 potential of a subset of Y_1R-expressing IC neurons. Thus, our data indicate that NPY neurons
80 represent a novel class of GABAergic IC principal neurons and that these neurons may use
81 GABAergic and NPY signaling to regulate the excitability of postsynaptic targets.
82

83 **Materials and Methods**

84 **Animals**

85 All experiments were approved by the University of Michigan Institutional Animal Care
86 and Use Committee and were in accordance with NIH guidelines for the care and use of

87 laboratory animals. Animals were kept on a 12-hour day/night cycle with ad libitum access to
88 food and water. NPY-hrGFP mice were obtained from Jackson Laboratory (stock # 006417; van
89 den Pol et al., 2009) and were maintained hemizygous for the hrGFP transgene by crossing with
90 C57BL/6J mice (Jackson Laboratory, stock # 000664). To visualize neurons that express Y_1R,
91 Npy1r^{cre} mice (B6.Cg-*Npy1r*$^{tm1.1(cre/GFP)Rpa}$/J, Jackson Laboratory, stock # 030544; Padilla et al.,
92 2016) were crossed with Ai14 Cre-reporter mice (B6.Cg-*Gt(ROSA)26Sor* $^{tm14(CAG-tdTomato)Hze}$,
93 Jackson Laboratory, stock # 007914). All mouse lines were on a C57BL/6J background. Because
94 C57BL/6J mice are subject to age-related hearing loss due to the *Cdh23*^{ahl} mutation (Noben-
95 Trauth et al., 2003), experiments were performed in animals aged P22 – P74, before the onset
96 of hearing loss symptoms at about 3 months of age.

97

98 **Analysis of the distribution of NPY neurons**

99 Three NPY-hrGFP mice were used to assess the distribution of NPY neurons in the IC.
100 Each hrGFP-expressing IC neuron was identified in a series of every third section through the
101 rostro-caudal extent of one IC. The locations of the labeled neurons were plotted using a
102 Neurolucida system (MBF Bioscience) attached to a Zeiss Axio Imager.Z2 microscope. IC
103 subdivisions were determined by examining staining for GAD67 and GlyT2 (Buentello et al.,
104 2015). Low magnification photomicrographs of the distribution of NPY neurons were collected
105 using a 5x objective on a Zeiss Axio Imager.Z2 microscope. Neurolucida Explorer was used to
106 export data to Excel for analysis.

107

108 **Immunohistochemistry**

109 Mice were deeply anesthetized and perfused transcardially with 0.1 M phosphate-
110 buffered saline (PBS), pH 7.4, for 1 min and then with a 10% buffered formalin solution
111 (Millipore Sigma, cat# HT501128) for 15 min. Brains were collected and post-fixed in the same
112 fixative for 2 hours and cryoprotected overnight at 4°C in 0.1 M PBS containing 20% sucrose.

113 Brains were cut into 40 µm sections on a vibratome or freezing microtome. Sections were
114 washed in 0.1 M PBS, and then treated with 10% normal donkey serum (Jackson
115 ImmunoResearch Laboratories, cat# 017-000-121, West Grove, PA) and 0.3% Triton X-100 for 2
116 hours. Sections were then incubated for 24 hours at 4 °C in mouse anti-GAD67 (1:1000;
117 Millipore Sigma, cat# MAB5406), rabbit anti-NeuN (1:500; Millipore Sigma, cat# ABN78), rabbit
118 Neuro-Chrom pan neuronal marker (1:1000; Millipore-Sigma, cat# ABN2300), rabbit anti-NPY
119 (1:1000; Peninsula Labs, cat# T-4070), guinea pig anti-GlyT2 (1:2000; Synaptic Systems cat#
120 272-004) or mouse anti-bNOS (1:1000, Millipore Sigma, cat#: N2280). On the following day,
121 sections were rinsed in 0.1 M PBS and incubated in Alexa Fluor 647-tagged goat anti-mouse IgG
122 or Alexa Fluor 750-tagged goat anti-rabbit IgG (1:100, Thermo Fisher, cat# A21235 and A21039),
123 or Alexa Fluor 647-tagged donkey anti-mouse IgG, Alexa Fluor 647-tagged donkey anti-rabbit
124 IgG, or Alexa Fluor 594-tagged goat anti-guinea pig IgG (1:500, Thermo Fisher, cat# A-21202, A-
125 21206 and A-11076) for 1.0 – 1.5 hours at room temperature. Sections were then mounted on
126 Superfrost Plus microscope slides (Thermo Fisher, cat# 12-550-15) and coverslipped using
127 Fluoromount-G (SouthernBiotech, cat# 0100–01) or DPX (Sigma-Aldrich cat# 06522). Images
128 were collected using a 1.30 NA 40x oil-immersion objective or a 1.40 NA 63x oil-immersion
129 objective on a Leica TCS SP8 laser scanning confocal microscope.

130

131 **Antibody validation**

132 All antibodies used in this study, except anti-NPY, have been previously validated in the
133 IC. To label GABAergic neurons, we used the mouse monoclonal anti-GAD67 antibody (Millipore
134 Sigma, cat# MAB5406). This antibody was raised against the 67 kDa isoform of glutamic acid
135 decarboxylase (GAD). The manufacturer reports that western blot analysis showed no cross-
136 reactivity with the 65 kDa isoform of GAD (GAD65). This antibody has been used in several
137 studies to identify GABAergic neurons in the IC (Ito et al., 2009; Mellott et al., 2014; Beebe et
138 al., 2016; Goyer et al., 2019). To identify neurons, we performed anti-NeuN staining with a
139 rabbit polyclonal antibody (Millipore Sigma, cat# ABN78). The manufacturer reports that anti-
140 NeuN specifically recognizes the DNA-binding, neuron-specific protein NeuN. Previous studies

141 used this antibody to identify neurons in the IC (Foster et al., 2014; Mellott et al., 2014; Beebe
142 et al., 2016; Goyer et al., 2019). To define the borders of IC subdivisions, we performed a
143 double staining using anti-GAD67 and anti-GlyT2 antibodies (Buentello et al., 2015). Guinea pig
144 anti-GlyT2 antibody (Synaptic Systems, cat# 272 004) was used to identify glycine transporter 2,
145 which is localized in axons. We also immunostained with anti-brain nitric oxide synthase (bNOS)
146 to define the borders of the IC subdivisions (Millipore Sigma, cat# N2280). This antibody was
147 raised against the IgG1 isotype from the NOS-B1 hybridoma. The manufacturer reports that
148 anti-bNOS reacts specifically with nitric oxide synthase (NOS), derived from brain (bNOS, 150 –
149 160 kDa). Previous studies used anti-bNOS to delineate the borders of IC subdivisions in guinea
150 pig and mouse (Coote and Rees, 2008; Keesom et al., 2018). Finally, to label NPY, we used the
151 polyclonal rabbit anti-NPY antibody (Peninsula Laboratories, cat# T-4070). Pretreatment with
152 antiserum containing NPY peptide abolished all staining, reinforcing the high specificity of this
153 antibody (Rowan et al., 1993). This antibody has been successfully used in cortex (Rose et al.,
154 2009; Milstein et al., 2015) and hippocampus (Ledoux et al., 2009).

155

156 **Analysis of GAD67 staining**

157 Analysis of GAD67 immunostaining was performed as previously reported (Goyer et al.,
158 2019). Images from representative sections of the IC (n = 2 male P74 mice, three sections per
159 mouse, one caudal, one medial and one rostral) were collected at 2 µm depth intervals with a
160 1.30 NA 40x oil-immersion objective on a Leica TCS SP8 laser scanning confocal microscope.
161 Images were analyzed using Leica LAS X software (version 3.3.0). As previously reported, anti-
162 GAD67 antibody did not penetrate the entire depth of the tissue sections (Beebe et al., 2016;
163 Goyer et al., 2019). For this reason, the analysis was restricted to the top 10 – 12 µm of each
164 section, where the antibody fully penetrated. Within this region, we manually marked every
165 hrGFP^{+} cell body in the left IC. We analyzed the green (hrGFP) and red (Alexa 647) channels
166 separately, so that labeling in one channel did not influence analysis of the other channel. After
167 the hrGFP cells were marked, the red and green color channels were merged, and in every
168 instance where a cell body contained markers for hrGFP, we evaluated if GAD67 was also

169 present. The number of double-labeled cells was compared to the total number of hrGFP$^+$
170 neurons to determine the percentage of hrGFP$^+$ neurons that were GAD67$^+$ as well.

171

172 **Analysis of NeuN staining with design-based stereology**

173 We used a design-based stereology approach to estimate the numbers of hrGFP$^+$ and
174 NeuN$^+$ neurons in brain sections that were stained with anti-NeuN antibody. This approach has
175 been previously described and validated in the IC (Goyer et al., 2019). In brief, we collected
176 systematic random samples using a virtual grid of 370 µm x 370 µm squares that was overlaid
177 on the IC section. The starting coordinates for the grid were set using the Mersenne Twister
178 random number generator in Igor Pro 7 or 8 (WaveMetrics Inc). We then collected images of
179 the coordinates determined by the upper-left intersection of each grid-square that fell over the
180 IC. Each image consisted of a 184 µm x 184 µm Z-stack collected at 1 µm depth intervals with a
181 1.40 NA 63x oil immersion objective on a Leica TCS SP8 confocal microscope. Eight to twenty
182 images were collected per slice. Three slices (caudal, middle and rostral) were analyzed per
183 mouse (n = 2). Using Neurolucida 360 (MBF Bioscience), we counted neurons using the optical
184 fractionator approach (West et al., 1991). In this approach, we defined guard zones as ≥2 µm-
185 thick regions at the top and bottom of the slice and excluded these from subsequent analysis.
186 Neurons between the guard zones, within a 15 µm-thick region at the center of the slice, were
187 counted by making a single mark at the top of each cell. Cells crossing the right and top borders
188 of the image stack were counted, whereas those crossing the left and bottom borders were
189 not. The red (NeuN) and green (hrGFP) color channels were analyzed separately, so that
190 labeling in one channel did not influence analysis of the other. In all neurons counted, hrGFP$^+$
191 cells were also NeuN$^+$ (1097/1097 cells). The total number of double-labeled (hrGFP$^+$/NeuN$^+$)
192 cells was then compared to the total number of NeuN$^+$ cells. We also collected tile scan images
193 of each IC section analyzed using a 10x objective and used GAD67 and GlyT2 staining to
194 determine the border separating the ICc from the IC shell (ICs) regions. The 63x Z-stacks were
195 aligned to these tile scans using Adobe Photoshop, and counted neurons were assigned to the
196 ICc or IC shell.

197

198 **Brain slice preparation**

199 To characterize the intrinsic physiology of NPY neurons and the effect of NPY on
200 neurons in the IC, whole-cell patch-clamp recordings were performed in NPY-hrGFP (van den
201 Pol et al., 2009) and Npy1r^{cre} mice (Padilla et al., 2016). Both males (n = 22) and females (n = 33)
202 aged P22 – P50 were used. No differences were observed between animals from different sexes
203 or ages (linear regression, p>0.05). Mice were deeply anesthetized with isoflurane and then
204 rapidly decapitated. The brain was removed, and the IC was dissected in ~34 °C artificial
205 cerebrospinal fluid (ACSF) containing (in mM): 125 NaCl, 12.5 glucose, 25 $NaHCO_3$, 3 KCl, 1.25
206 NaH_2PO_4, 1.5 $CaCl_2$, 1 $MgSO_4$, 3 sodium pyruvate and 0.40 L-ascorbic acid, bubbled to a pH of
207 7.4 with 5% CO_2 in 95% O_2. Coronal sections of the IC (200 µm) were cut in ~34 °C ACSF with a
208 vibrating microtome (VT1200S, Leica Biosystems) and incubated at 34 °C for 30 min in ACSF
209 bubbled with 5% CO_2 in 95% O_2. After incubation, slices were placed at room temperature for
210 at least 30 min before being transferred to the recording chamber. All chemicals were obtained
211 from Thermo Fisher Scientific unless otherwise noted.

212

213 **Electrophysiological recordings**

214 For recordings, slices were placed into a chamber that was continuously perfused at ~2
215 ml/min with 34°C oxygenated ACSF. NPY-hrGFP neurons and Y_1R-tdTomato neurons in IC slices
216 were identified with epifluorescence using a Nikon FN1 microscope. Whole-cell current-clamp
217 recordings were performed with a BVC-700A patch clamp amplifier (Dagan Corporation). Data
218 were low-pass filtered at 10 kHz, sampled at 50 kHz with a National Instruments PCIe-6343 data
219 acquisition board, and acquired using custom software written in IgorPro.

220 Recording pipettes were pulled from borosilicate glass pipettes (outer diameter 1.5 mm,
221 inner diameter 0.86 mm, cat# BF150-86-10, Sutter Instrument) using a P-1000 microelectrode
222 puller (Sutter Instrument). Pipettes were filled with an internal solution containing (in mM): 115
223 K-gluconate, 7.73 KCl, 0.5 EGTA, 10 HEPES, 10 Na_2phosphocreatine, 4 MgATP, 0.3 NaGTP,

224 supplemented with 0.1% biocytin (w/v), pH adjusted to 7.3 with KOH and osmolality to 290
225 mmol/kg with sucrose. Pipettes with resistances of 3.0 - 4.8 MΩ when filled with internal
226 solution were used for recordings.

227 Input resistance was assessed by applying a series of 100 ms current steps that
228 hyperpolarized the membrane potential from just below rest to < −100 mV. For each step
229 response, the peak and steady-state voltage changes were measured, and these values were
230 used to generate voltage versus current plots from which the peak (R_{pk}) and steady-state (R_{ss})
231 input resistances were calculated based on the slope of a linear regression. Membrane time
232 constant was determined by applying fifty, 300 ms current steps that hyperpolarized the
233 membrane potential by 2 - 4 mV and taking the median of the time constants obtained by
234 fitting an exponential function to each response. All membrane potential values were corrected
235 for the liquid junction potential (-11 mV). Capacitance and series resistance were compensated
236 using bridge balance. Recordings with series resistance >20 MΩ or changes in series resistance
237 >15% during the recording period were discarded.

238 To test if NPY neurons are pacemaker neurons (n = 8), we blocked synaptic inputs using
239 50 µM D-AP5 (NMDA receptor antagonist, Hello Bio, cat# HB0225) and 10 µM NBQX disodium
240 salt (AMPA receptor antagonist, Hello Bio, cat# HB0443). All drugs were diluted in standard
241 ACSF.

242 To evaluate the effects of Y_1R activation, Y_1R-tdTomato neurons were targeted for
243 recordings. Since most NPY neurons spontaneously fire (n = 87 out of 121 cells), we included 1
244 µM tetrodotoxin (TTX, Hello Bio, cat# HB1035) in the ACSF in this experiment to block action
245 potential mediated release of NPY. In current clamp mode, Y_1R neurons were held for 10 min
246 before starting the control period recording to limit possible effects of intracellular dialysis.
247 During these 10 min, R_{pk}, R_{ss} and membrane time constant were collected to monitor the health
248 of the neuron. At the start of the 5 min control period, we initiated a protocol that recorded the
249 resting membrane potential (V_{rest}) every 10 seconds. Only neurons with a stable V_{rest} , defined
250 as V_{rest} drift <3 mV, were included in the analysis. We then applied 500 nM [Leu^{31}, Pro^{34}]-NPY
251 (Tocris, cat # 1176), a high affinity Y_1R agonist. We used 500 nM [Leu^{31}, Pro^{34}]-NPY based on

252 previous studies performed in the hypothalamus (Roa and Herbison, 2012) and hippocampus
253 (Giesbrecht et al., 2010). [Leu^{31}, Pro^{34}]-NPY was diluted in 10 ml of ACSF and bath applied for ~5
254 min. The recording was then continued for a 20 - 50 min washout period. Only neurons that
255 had a washout period over 20 min were included in the analysis. Control experiments followed
256 the same approach, using a vehicle solution (normal ACSF).

257 To analyze the effect of [Leu^{31}, Pro^{34}]-NPY on the V_{rest} of IC neurons, we compared V_{rest}
258 during the final two min of the baseline period with the initial 2 min of the drug application
259 period (see Figure 7B, C, gray bars). The drug application period started 90 s after the end of the
260 control period to allow time for the drug solution to reach the recording chamber. A cell was
261 considered sensitive to [Leu^{31}, Pro^{34}]-NPY if it exhibited a >2 mV change in V_{rest} compared to
262 baseline.

263

264 **Post hoc reconstructions of morphology and morphology analysis**

265 Neurons were filled with biocytin via the recording pipette. After the recording, an
266 outside-out patch was formed, by slowly removing the pipette, to allow the cell membrane to
267 reseal. Brain slices were then fixed overnight in 4% paraformaldehyde (PFA) in 0.1 M phosphate
268 buffer (PB, pH 7.4) and moved to 0.1 M PBS the next day. Slices were stored at 4 °C for up to
269 three weeks and then stained using fluorescent biocytin-streptavidin histochemistry. For this,
270 slices were washed in 0.1 M PBS three times for 10 min (3 × 10 min in PBS), the membrane was
271 permeabilized in 0.2% Triton X-100 in 0.1 M PBS for 2 hours, washed 3 × 10 min in PBS, and
272 stained at 4 °C for 24 hours with streptavidin-Alexa Fluor 647 (1:1000). The next day, slices
273 were washed 3 × 10 min with PBS, post fixed in 4% paraformaldehyde (PFA) in 0.1 M phosphate
274 buffer (PB, pH 7.4) for 1 hour and then washed 3 × 10 min with PBS. Slices were then mounted
275 on Superfrost Plus microscope slides in anti-fade media (Fluoromount-G). Images were
276 obtained with a Leica TCS SP8 laser scanning confocal microscope using a 1.40 NA 63x oil-
277 immersion objective. Z-stack tile scans were performed to image the soma and dendritic arbor.
278 Image stacks were imported into Neurolucida 360 (MBF Bioscience), where three-dimensional
279 reconstructions and quantitative analyses of neuronal morphology were performed.

280

281 **Intracranial virus injections**

282 To evaluate the axonal projections of NPY neurons, we used the "Cre recombinase
283 dependent on GFP" (Cre-DOG) system to selectively express Cre recombinase in GFP expressing
284 neurons (Tang et al., 2015) in the IC of NPY-hrGFP mice. For this, NPY-hrGFP mice were injected
285 in the right IC with a mixture of three viruses: a Cre-dependent tdTomato virus,
286 rAAV2/1.CAG.LSL.tdTomato (Addgene # 100048; titer = 1.10 x 10^{13} gc/ml), and the two AAVs
287 needed for Cre-DOG, rAAV2/1-EF1a-N-CretrcintG (Addgene # 69570; titer = 8.223 x 10^{13} gc/ml)
288 and rAAV2/1-EF1a-C-CreintG (Addgene # 69571; titer = 8.227 x 10^{13} gc/ml). The latter two of
289 these viruses produce two halves of a split Cre-GFP binding protein that assemble in the
290 presence of GFP to produce functional Cre recombinase.

291 Surgeries were performed on males and females, aged P21 – P24, using standard aseptic
292 techniques. Mice were deeply anesthetized with isoflurane (2 – 3%) and their body
293 temperature maintained with a homeothermic heating pad. The analgesic carprofen (5 mg/kg,
294 CarproJect, Henry Schein Animal Health) was injected subcutaneously. The scalp was shaved
295 and a rostro-caudal incision was made along the midline to expose the skull. A unilateral
296 craniotomy was performed over the right IC, using a micromotor drill (K.1050, Foredom Electric
297 Co.) with a 0.5 mm burr (Fine Science Tools). Injection sites were defined using stereotaxic
298 coordinates relative to the lambda suture, with injection depths relative to the surface of the
299 skull at lambda. Injections were made in two penetrations: penetration 1 – 900 µm caudal,
300 1000 µm lateral, and 2000 µm deep; penetration 2 – 900 µm caudal, 1250 µm lateral, and 2000
301 µm deep. One injection of 50 - 60 nl of virus was performed in each penetration, resulting in
302 two virus deposits with a total volume of 100 -120 nl. Viral constructs were injected with a
303 NanoJect III nanoliter injector (Drummond Scientific Company) connected to a MP-285
304 micromanipulator (Sutter Instruments). Glass injection pipettes were pulled using 1.14 mm
305 outer diameter, 0.53 mm inner diameter capillary glass (cat# 3-000-203-G/X, Drummond
306 Scientific Company) with a P-1000 microelectrode puller (Sutter Instrument). The injector tip
307 was cut and then beveled at 30° with a BV-10 pipette beveller (Sutter Instrument). Injectors

308 were back-filled with mineral oil and then front-filled with virus. After the injections were
309 complete, the scalp was sutured, using Ethilon 6–0 (0.7 metric) nylon sutures (Ethicon USA LLC),
310 and the incision was treated with 0.5 ml 2% Lidocaine hydrochloride jelly (Akorn Inc.). After
311 recovery from anesthesia, mice were returned to the vivarium and were monitored daily until
312 the wound healed. After allowing 3 – 4 weeks for protein expression, mice were perfused and
313 axonal projections were analyzed.

314

315 **Subdivisions of the IC**

316 We used two different approaches to define the borders between the ICc, ICd, and IClc.
317 For the stereology experiments and for the analysis of the distribution of NPY neurons,
318 subdivision borders were defined using a combination of GlyT2 and GAD67 staining (Buentello
319 et al., 2015). To identify the subdivisions in which reconstructed neurons were located, we used
320 bNOS staining (Coote and Rees, 2008). Both methods have been previously validated in the IC,
321 and we did not observe any obvious difference between the subdivision borders obtained with
322 these approaches.

323

324 **Analysis of axonal projections**

325 Axonal projections of NPY neurons were analyzed in 11 NPY-hrGFP mice that received
326 intracranial injections of Cre-DOG and FLEX-tdTomato viruses. Neurons expressing tdTomato
327 were present in one IC in all but one case. Injection sites were characterized by neurons filled
328 with tdTomato that also expressed hrGFP. In each case, the brain was examined for tdTomato-
329 expressing axons and boutons, which were assumed to originate from NPY neurons in the
330 injected IC. In some cases, the injection site encroached on the ventral IC border, but
331 tdTomato-expressing axons and boutons were present in substantial numbers in each of the
332 major projection targets reported here in every case, including those where the injection site
333 was restricted to the IC. Staining for NeuN and Neuro-Chrom was used to identify target nuclei.
334 Low magnification images of the injection site were taken using a 5x objective on a Zeiss

335 AxioImager.Z2 microscope. High magnification images of neurons at the injection site and of
336 tdTomato-labeled axons and boutons were collected as z-stacks using a 63x oil-immersion
337 objective (NA = 1.4) on a Zeiss Axio Imager.Z2 microscope using structured illumination
338 (Apotome 2, with 0.5 µm z-step interval) to provide optical sectioning. Presented images are
339 maximum projections of collected stacks.

340

341 **Statistics**

342 All statistical analyses were performed in Igor Pro. Data are presented as mean ± SD.
343 The statistical tests used for each experiment are indicated in the results. Results were
344 considered significant when $P < 0.05$.

345

346 **Results**

347 **NPY neurons are distributed throughout the main subdivisions of the IC**

348 To target experiments to NPY-expressing neurons, we obtained the NPY-hrGFP mouse
349 line, in which hrGFP expression is driven by the NPY promoter (van den Pol et al., 2009). Figure
350 1 shows that hrGFP-labeled cells are present throughout the rostro-caudal extent of the IC in
351 these mice. We performed immunostaining against the NPY peptide to determine whether this
352 mouse line selectively labels NPY-expressing neurons in the IC. In brain slices from two P58
353 males, we counted hrGFP$^+$ neurons in one caudal, one middle and one rostral section of the IC
354 per animal (n = 3205 hrGFP$^+$ neurons, Figure 2A-C). We then evaluated whether each hrGFP$^+$
355 neuron co-labeled with anti-NPY. We found that 94.7% of hrGFP$^+$ neurons were NPY$^+$, indicating
356 that the NPY-hrGFP mouse line provides highly selective labeling of NPY-expressing neurons (n
357 = 3035 hrGFP$^+$/NPY$^+$ neurons and 170 hrGFP$^+$/NPY$^-$ neurons, Table 1).

358

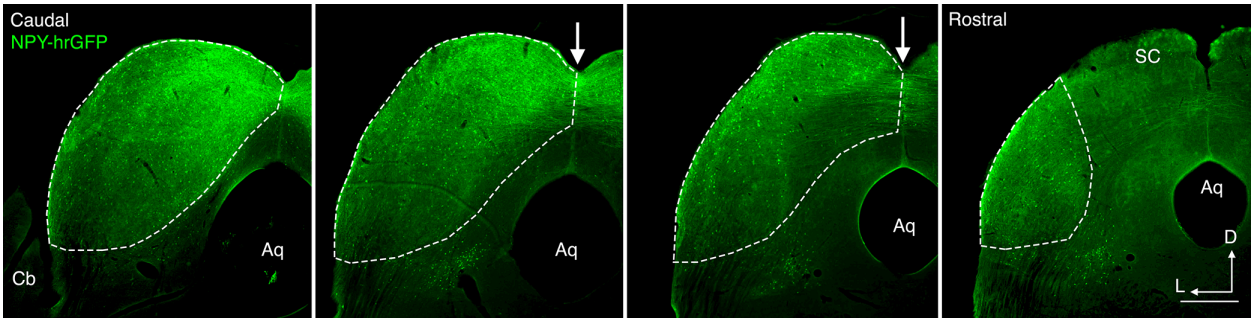

Figure 1. NPY neurons are distributed throughout the IC. Micrographs of a series of coronal sections through the IC of an NPY-hrGFP mouse. NPY$^+$ cells (green) were observed in all sections through the IC, but were more numerous caudally, especially in the dorsomedial aspects of these sections. White arrows indicate NPY$^+$ axons crossing the IC commissure. Aq- cerebral aqueduct, Cb- cerebellum, SC- superior colliculus. Scale bar = 500 µm.

NPY neurons represent one-third of the GABAergic neurons in the IC

NPY neurons are nearly exclusively GABAergic in the cerebral cortex (Karagiannis et al., 2009), hippocampus (Milner et al., 1997) and hypothalamus (Henry et al., 2015; Marshall et al., 2017). To investigate the neurotransmitter content of NPY neurons in the IC, we performed immunostaining against GAD67, an enzyme essential for GABA synthesis. Using brain slices from two P74 males (Figure 2D-F), we counted hrGFP$^+$ neurons in one caudal, one middle and one rostral section of the IC per animal (n = 2673 hrGFP$^+$ neurons). We then determined whether each hrGFP$^+$ neuron co-labeled with anti-GAD67. Out of the 2673 hrGFP$^+$ neurons counted, 98.5% were GAD67$^+$ (n = 2633 hrGFP$^+$/GAD67$^+$ neurons and 40 hrGFP$^+$/GAD67$^-$ neurons, Table 1). We suspect that the absence of GAD67 immunostaining in 40 hrGFP$^+$ neurons was due to rare cases of poor antibody penetration or nonspecific expression of hrGFP. Thus, these data indicate that NPY neurons in the IC are GABAergic.

Next, we used design-based stereology to determine the percentage of neurons in the IC that express NPY. For this experiment, we analyzed the ICc and IC shell (ICs = ICd plus IClc) separately, defining the borders between these subdivisions according to the pattern of GAD67 and GlyT2 immunoreactivity (Buentello et al., 2015). Sections from two P54 male NPY-hrGFP

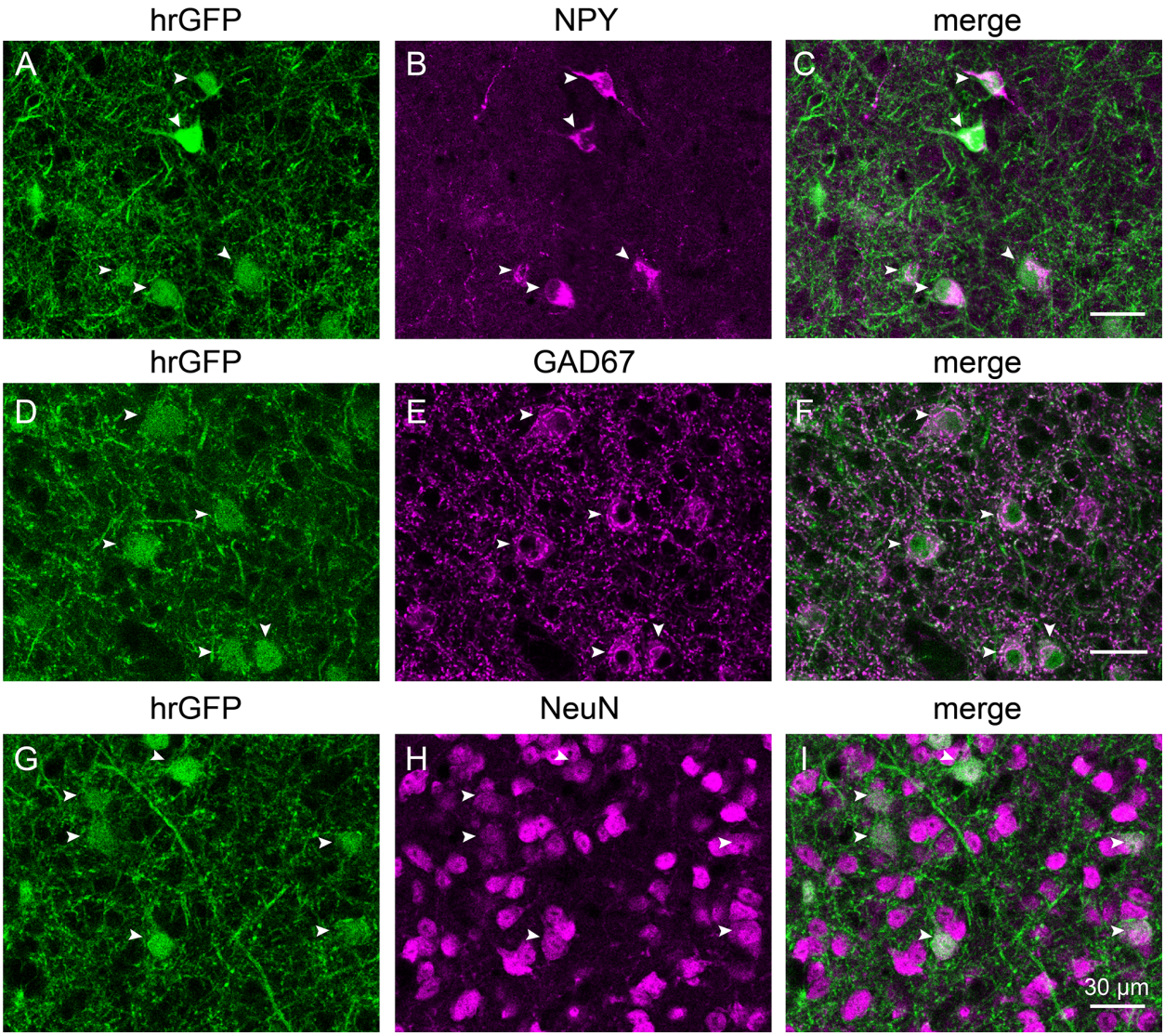

Figure 2. NPY neurons express NPY, are GABAergic, and represent 7.6% of neurons in the ICc. ***A, D, G,*** Confocal images of NPY neurons expressing hrGFP in coronal sections of the ICc from NPY-hrGFP mice. ***B,*** Confocal images showing immunostaining for NPY (magenta). ***C,*** Nearly all hrGFP$^+$ neurons colocalized with anti-NPY. ***E,*** Confocal images showing immunostaining for GAD67 (magenta). ***F,*** Nearly all hrGFP$^+$ neurons were positive for GAD67 (magenta). ***H,*** Confocal images showing immunostaining for NeuN (magenta). ***I,*** All NPY neurons were positive for NeuN. White arrowheads indicate NPY neurons labeled by NPY, GAD67 and NeuN. Scale bar = 30 µm, applies to all images.

mice were stained with anti-NeuN, a neuron-selective antibody previously shown to label most or all neurons in the IC (Mellott et al., 2014; Beebe et al., 2016). Three sections per mouse were analyzed: one caudal, one middle, and one rostral. To ensure unbiased counting of neurons, we applied the optical fractionator method (see Materials and Methods). Sections adjacent to the

395 **Table 1. NPY neurons express NPY and are GABAergic.**

Animal	Slice #	# hrGFP$^+$	# NPY$^+$	# hrGFP$^+$ NPY$^-$	% hrGFP$^+$ NPY$^+$
P58 male #1	1 (caudal)	464	436	28	94.0
	2 (middle)	563	537	26	95.4
	3 (rostral)	567	537	30	94.5
	Total	**1594**	**1510**	**84**	**94.7**
P58 male #2	1 (caudal)	496	485	11	97.8
	2 (middle)	602	555	47	92.2
	3 (rostral)	514	486	28	94.6
	Total	**1612**	**1526**	**86**	**94.7**
Grand total		**3206**	**3036**	**170**	**94.7**
Average across two mice					**94.7**

396

Animal	Slice #	# hrGFP+	# GAD67+	# hrGFP$^+$ GAD67-	% hrGFP$^+$ GAD67$^+$
P74 male #1	1 (caudal)	456	450	6	98.7
	2 (middle)	387	380	7	98.2
	3 (rostral)	328	322	6	98.2
	Total	**1171**	**1152**	**19**	**98.4**
P74 male #2	1 (caudal)	468	462	6	98.7
	2 (middle)	346	337	9	97.4
	3 (rostral)	688	682	6	99.1
	Total	**1502**	**1481**	**21**	**98.6**
Grand total		**2673**	**2633**	**40**	**98.5**
Average across two mice					**98.5**

397

398 anti-NeuN sections were immunostained with anti-GAD67 and anti-GlyT2, and IC subdivision
399 boundaries were determined by comparing these to the adjacent anti-NeuN stained sections.
400 This analysis showed that NPY neurons represented 7.6% of neurons in the ICc and 7.8% in the
401 ICs (Table 2). Since previous studies indicate that 20 – 27% of IC neurons are GABAergic (Oliver
402 et al., 1994; Merchán et al., 2005; Beebe et al., 2016), our results suggest that NPY-expressing
403 neurons account for approximately one-third (27 – 39%) of GABAergic neurons in the IC.

404

405

406 **Table 2. NPY neurons represent 7.6% of neurons in the ICc and 7.8% of neurons in the ICs.**

ICc				
Coronal Slice	**P58 Male #1**	**P58 Male #2**	**Per slice pane**	**Grand average**
Caudal	8.0% (60/755) 7 samples	9.4% (15/159) 4 samples	8.2% (75/914) 11 samples	
Medial	7.9% (84/1070) 11 samples	7.0% (90/1278) 9 samples	7.4% (174/2348) 20 samples	
Rostral	7.7% (77/999) 10 samples	7.2% (68/942) 10 samples	7.5% (145/1941) 20 samples	
Per mouse	7.8% (221/2824)	7.3% (173/2379)		7.6% (394/5203)

ICs				
Coronal Slice	**P58 Male #1**	**P58 Male #2**	**Per slice pane**	**Grand average**
Caudal	8.6% (140/1620) 12 samples	6.3% (29/460) 7 samples	8.1% (169/2080) 19 samples	
Medial	6.9% (128/1849) 11 samples	10.4% (76/728) 8 samples	7.9% (204/2577) 19 samples	
Rostral	8.3% (55/668) 12 samples	6.7% (77/1155) 11 samples	7.2% (132/1823) 23 samples	
Per mouse	7.8% (323/4137)	7.8% (182/2343)		7.8% (505/6480)

407

408 Together, the above data show that NPY is expressed in a population of GABAergic
409 neurons in the IC, but do not indicate whether this population represents one or several neuron
410 types. To test this, we next analyzed the physiological and morphological properties of NPY
411 neurons.

412

413 **Most NPY neurons exhibit a sustained firing pattern and have a propensity to spontaneously**
414 **fire**

415 In acute brain slices, we targeted whole-cell current clamp recordings to NPY-hrGFP
416 neurons in the Icc, Icd, and Iclc. The location of the recording was noted at the end of the
417 recording and confirmed during retrieval of neuronal morphology (morphology was recovered
418 from 50 out of 146 recorded neurons). Because the intrinsic physiology of NPY neurons did not
419 differ across IC subdivisions, neurons from Icc, Icd, and Iclc are lumped together here. Most NPY
420 neurons presented moderate voltage sag in response to hyperpolarizing current steps (Figure
421 3A, left) and a sustained firing pattern in response to depolarizing current steps (Figure 3A,
422 right). Firing versus current functions were determined with 1 s depolarizing current steps and
423 showed that NPY neurons had relatively linear input-output functions (Figure 3B). NPY neurons
424 had an average resting membrane potential of -63.4 ± 3.8 mV (Figure $3C_1$) and exhibited
425 relatively low expression of I_h current, with voltage sag ratios (steady-state/peak) of 0.89 ± 0.09
426 and 0.90 ± 0.09 measured from current steps that elicited peak hyperpolarization of -91.1 ± 1.8
427 mV and -111.0 ± 0.7 mV, respectively (Figure C_2). In addition, NPY neurons exhibited moderate
428 membrane time constants (15.9 ± 8.6 ms, Figure $3C_3$) and input resistances (R_{pk} = 238.7 ± 124.0
429 MΩ, R_{ss} = 249.5 ± 167.0 MΩ, Figure $3C_4$) and cells that did not spontaneously fire had low
430 rheobase values (46.7 ± 25.1 pA, Figure $3C_5$).

431 Neurons were classified as having a sustained firing pattern if their spike frequency
432 adaptation ratio (SFA ratio, last interspike interval/first interspike interval) was less than 2 and
433 as adapting if their SFA ratio was greater than 2 (Peruzzi et al., 2000). We found that 92.4% of
434 NPY neurons (n = 135 out of 146) had a sustained firing pattern in response to current steps
435 that elicited ~5 spikes and 89.7% (n = 96 out of 107) had a sustained firing pattern in response
436 to current steps that elicited ~10 spikes (Figure $3C_6$). Because neurons in the IC exhibit diverse
437 firing patterns, the finding that nearly all NPY neurons had sustained firing patterns supports
438 the hypothesis that NPY neurons constitute a distinct neuron class.

439 Interestingly, 71.9% of NPY neurons fired spontaneously at rest, with a median firing
440 rate of 0.22 Hz (n = 87 out of 121 neurons, range: 0.01 – 28.06 Hz, mean = 2.70 Hz; Figure 3D).

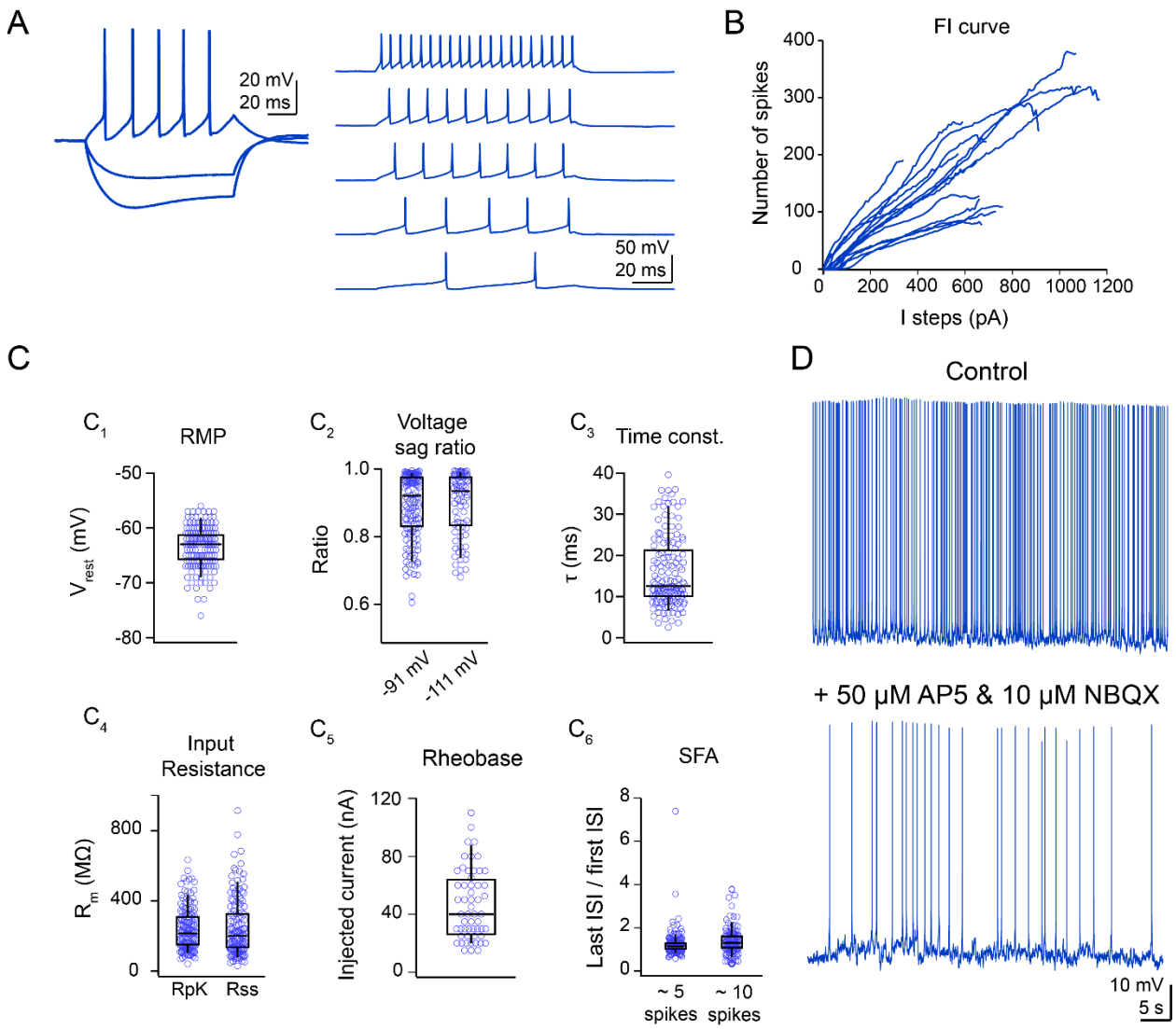

Figure 3. NPY neurons have a sustained firing pattern and most fire spontaneously. *A,* NPY neurons exhibited a sustained firing pattern in response to depolarizing current steps and a moderate voltage sag in response to hyperpolarizing current steps. ***B,*** Firing vs input analysis showed a linear input-output response, with increasing firing rates in response to increasingly large depolarizing current steps. Example FI curves from 15 neurons are shown. ***C,*** NPY neurons exhibited moderate intrinsic physiological properties. ***C_1,*** resting membrane potential, ***C_2,*** voltage sag ratio, ***C_3,*** membrane time constant, ***C_4,*** input resistance, ***C_5,*** rheobase, and ***C_6,*** spike frequency adaptation ratio. Boxplots show median, 25th and 75th percentile (box), and 9th and 91st percentile (whiskers). ***D,*** Most NPY neurons spontaneously fired at rest, and spontaneous firing persisted in 7 out of 8 cells in the presence of synaptic blockers (50 μM D-AP5 and 10 μM NBQX).

To determine whether spontaneous firing was driven by spontaneous synaptic input, we applied 50 μM D-AP5 and 10 μM NBQX to block AMPA and NMDA receptors and found that spontaneous firing remained in 7 out of 8 neurons (Figure 3D). These results suggest that NPY

456 neurons possess an intrinsic pacemaker ability, which may enable NPY neurons to provide tonic
457 GABAergic and NPY tone in the IC.

458

459 **NPY neurons have stellate morphology**

460 Using biocytin-streptavidin staining, we reconstructed the morphology of 49 NPY
461 neurons. Twenty-four of these neurons were located in the ICc, 18 in ICd and 7 in IClc. Figure 4
462 shows examples of the morphology of NPY neurons in the ICc, ICd and IClc. For comparison
463 purposes, neurons are oriented as they would appear in a coronal section of the left IC viewed
464 from a caudal perspective. Visual inspection suggested that NPY neurons had a stellate
465 morphology in all subdivisions. This is expected for ICd and IClc, where most neurons are
466 stellate, but in the ICc, only 15 - 20% of neurons have stellate morphology (Oliver and Morest,
467 1984; Oliver et al., 1991).

468 We used several quantitative approaches to test whether the dendritic arbors of NPY
469 neurons in the ICc were consistent with the stellate morphology predicted by visual inspection.
470 First, we used two-dimensional principal component analysis (PCA) to determine the
471 orientation and extent of the “length” (first principal direction) and “width” (second principal
472 direction) axes of each NPY neuron within the coronal plane (Figure 5A). In the mouse, the
473 isofrequency laminae extend at a ~40° - 50° angle relative to the horizontal plane, and it is
474 expected that the long axis of disc-shaped neurons extends parallel to the isofrequency laminae
475 (Stiebler and Ehret, 1985). Our data show that the long axis of NPY neurons in the ICc did not
476 have a preferred orientation, and only 3 of 24 neurons had a long axis oriented between 30°
477 and 60° (Figure 5B).

478 Second, because the dendrites of ICc stellate neurons typically extend across more than
479 one isofrequency lamina, we measured how far ICc NPY neurons extended their dendrites
480 perpendicular to a 45° laminar plane. Although the width of isofrequency laminae has not been

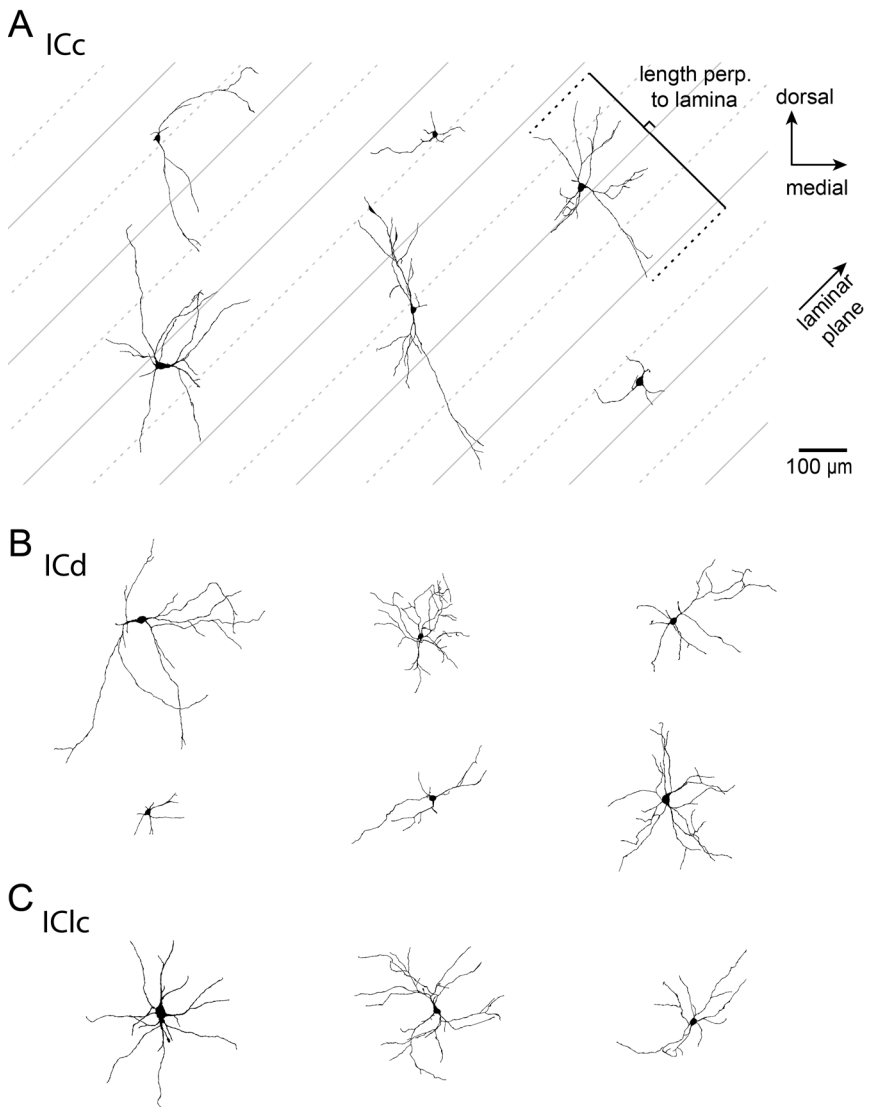

481

482 **Figure 4. Morphology of NPY neurons in the ICc, ICd, and IClc.** Representative reconstructions of the
483 morphology of 6 NPY neurons from the ICc (***A***), 6 NPY neurons from the ICd (***B***), and 3 NPY neurons from
484 the IClc (***C***). The gray lines in the ICc representation were drawn to illustrate the approximate orientation
485 and spacing of the isofrequency laminae (45° angle). Solid gray lines are spaced 200 µm apart, dashed
486 lines and solid lines are spaced 100 µm apart.

487

488 determined in mice, the distance between laminae in rats presumably provides a conservative
489 estimate for mice and ranges between 90 µm and 150 µm (Malmierca et al., 1993). We found
490 that only 4 out of 24 ICc NPY neurons had dendritic arbors that extended <90 µm perpendicular
491 to the laminar plane, and only 9 out of 24 had dendrites that extended <150 µm perpendicular

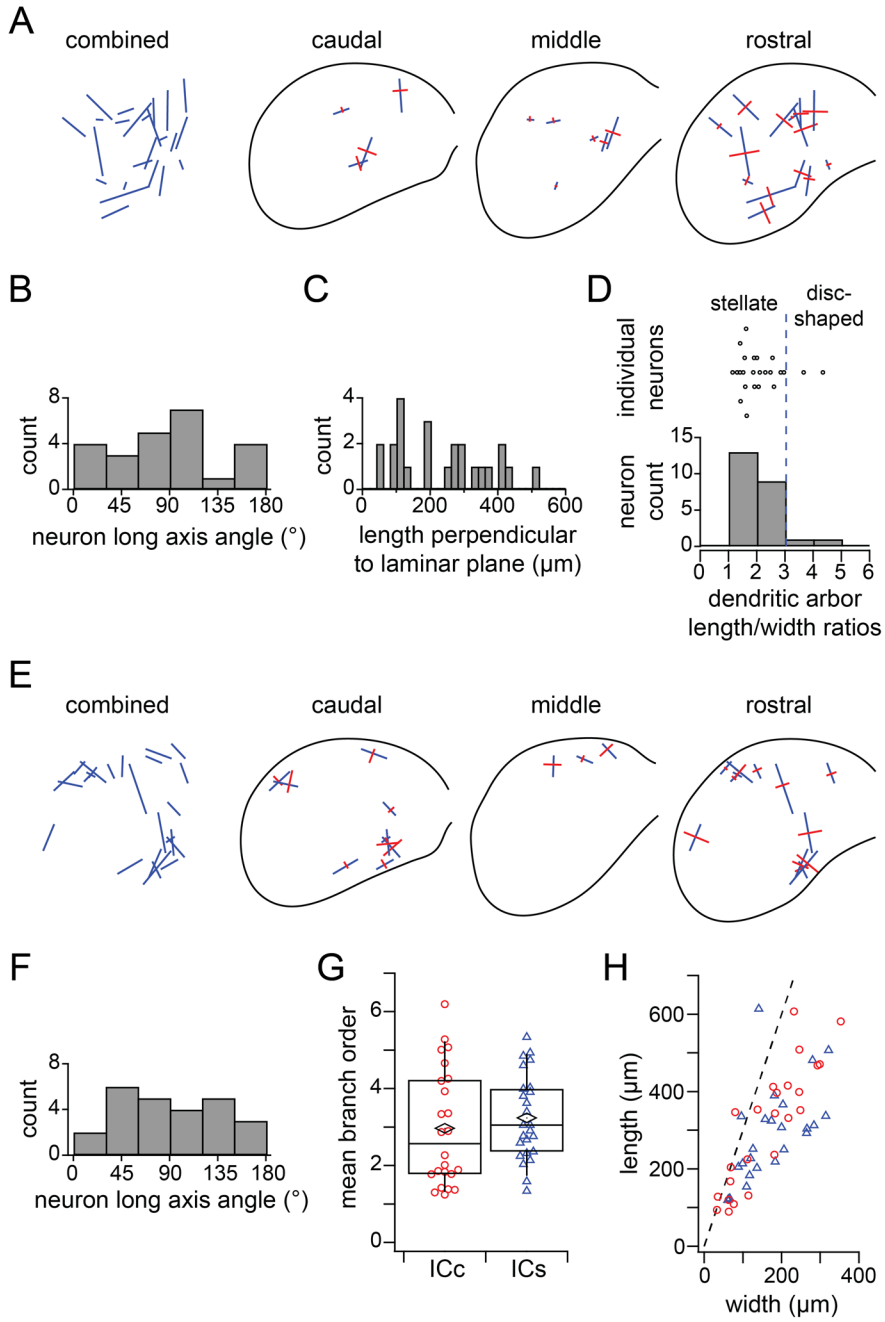

492

493 **Figure 5. NPY neurons are a class of stellate cells. *A*,** Orientation of the dendritic arbors of NPY neurons
494 from the ICc. Combined: all reconstructed neurons from the ICc (n = 24). Blue lines indicate the
495 orientation and length of the longest axis (first principal direction) of each neuron determined using 2D
496 PCA. Caudal, middle and rostral: orientation of dendritic fields separated according to position along the
497 rostro-caudal axis of the ICc. Blue lines indicate longest axis, perpendicular red lines indicate second
498 longest axis (second principal direction) as determined by 2D PCA. ***B*,** Angular orientation of the long axis
499 for every reconstructed NPY neuron located in the ICc. Angles indicate counter-clockwise rotation
500 relative to the medial-lateral (horizontal) axis. ***C*,** Extent of dendritic arbors of ICc NPY neurons
501 perpendicular to the plane of the isofrequency laminae (45°). ***D*,** 3D PCA was used to determine the
502 length and width axes of NPY neurons in the ICc. 92% (22 out of 24) of NPY neurons had a length to

503 width ratio <3, indicating that they are stellate cells. ***E,*** Orientation of the dendritic fields of NPY neurons
504 from the ICd and IClc (combined as ICs). Colors of lines and arrangement of sections are the same as in
505 ***A***. ***F,*** Angular orientation of the long axis for every reconstructed NPY neuron located in the ICs (n = 25).
506 Angles indicate counter-clockwise rotation relative to the medial-lateral (horizontal) axis. ***G,*** Comparison
507 of the mean dendritic branch order between NPY neurons in the ICc and ICs. ***H,*** Comparison of the
508 length/width ratio between NPY neurons in the ICc and ICs. The dashed line indicates length/width ratio
509 = 3.

510

511 to the laminar plane (Figure 5C). This suggests that the majority of ICc NPY neurons have
512 dendritic arbors that extend across two or more isofrequency laminae.

513 Third, we performed three-dimensional principal component analysis on the x, y, z
514 coordinate set for each ICc NPY neuron to determine the length (extent along the first principal
515 direction) and width (extent along the second principal direction) of each neuron in three
516 dimensions. We then calculated the length-to-width ratio of the dendritic arbor. Oliver and
517 colleagues showed that stellate neurons have a length-to-width ratio <3 and disc-shaped
518 neurons have a ratio $\geq$ 3 (Oliver et al., 1991). We found that 22 out of 24 NPY neurons (92%) in
519 the ICc had a length to width ratio < 3, consistent with the hypothesis that NPY neurons are
520 stellate (Figure 5D). Combined, the above quantitative analyses support the conclusion that ICc
521 NPY neurons are a class of stellate cells. Because stellate cells represent 15 – 20% of ICc
522 neurons (Oliver and Morest, 1984; Oliver et al., 1991) and our stereology data (Figure 2 G-I)
523 indicate that NPY neurons represent 7.6% of neurons in the ICc, NPY neurons represent 38 -
524 50% of stellate neurons in the ICc.

525 We also performed two-dimensional principal component analysis on NPY neurons
526 located in the ICd and IClc (combined as ICs; Figure 5E). As in the ICc, the longest axis of NPY
527 neurons in the ICs did not exhibit a preferred orientation (Figure 5F). Instead, the long axes of
528 ICs NPY neurons appeared to run parallel to the outer edge of the IC. Next, we compared the
529 morphology of NPY neurons in the ICc versus those in the ICs. Interestingly, no difference was
530 observed in the mean branch order number (ICc: 3.11 ± 1.54; ICs: 3.11 ± 1.04; two-tailed Mann-
531 Whitney-Wilcoxon test, p = 0.713; Figure 5G) or the dendritic length/width ratio (ICc: 2.16 ±

532 0.87; ICs: 1.74 ± 0.55; two-tailed Mann-Whitney-Wilcoxon test, p = 0.091; Figure 5H). Thus,
533 there were no gross morphological differences between NPY neurons in the ICc and ICs.

534

535 **NPY neurons project to auditory thalamus and other targets**

536 To examine the projections of NPY neurons in the IC, we made injections of AAV-Cre-
537 DOG and AAV-FLEX-tdTomato into the IC unilaterally in NPY-hrGFP mice. The combination of
538 these viruses allows Cre expression in cells expressing GFP (here, NPY cells), and subsequent
539 tdTomato expression in those Cre-expressing cells. In this way, we were able to use tdTomato
540 expression to identify axons and boutons throughout the brainstem that originate in NPY
541 neurons of the IC. An example of an injection site is shown in Figure 6A. Note that hrGFP

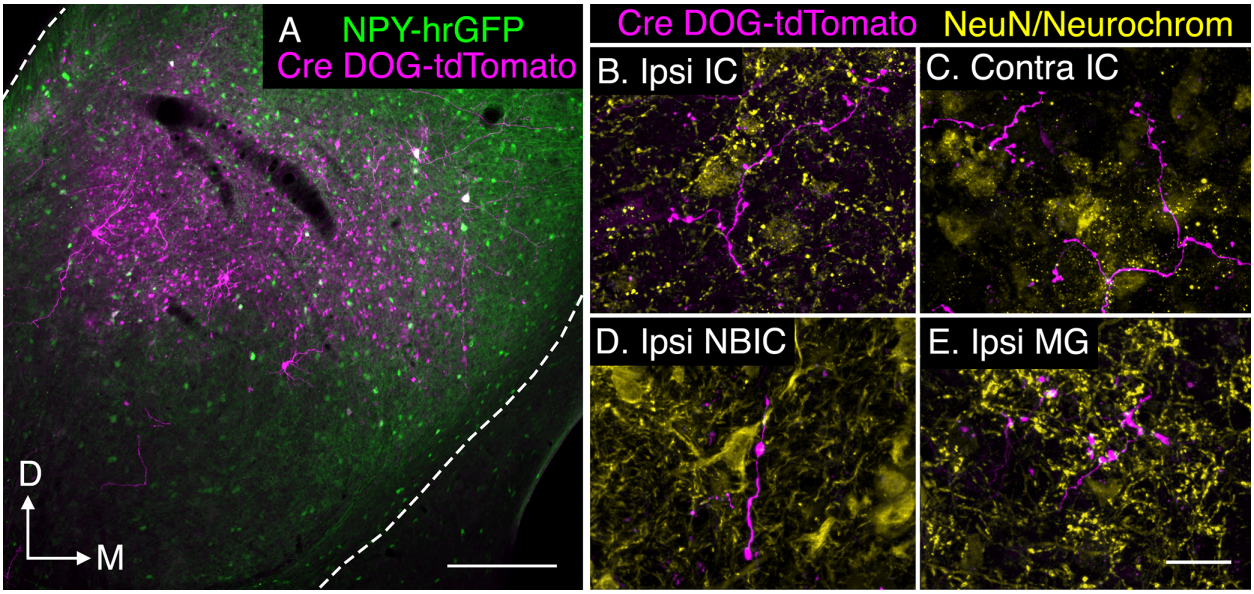

542

543 **Figure 6. NPY neurons send GABAergic projections to several long-range targets. *A,*** Micrograph of an
544 rAAV injection site in the IC of an NPY-hrGFP mouse. The IC was injected with rAAVs for the Cre-DOG
545 system and Cre-dependent tdTomato, resulting in tdTomato expression in transfected NPY neurons
546 (magenta). hrGFP expression is shown in green. Scale bar = 250 µm. ***B-E,*** Higher magnification micrographs
547 show tdTomato$^+$ axons and boutons from IC NPY neurons (magenta) terminating in four brain regions:
548 ipsilateral IC, contralateral IC, ipsilateral nucleus of the brachium of the IC (NBIC), and ipsilateral medial
549 geniculate nucleus (MG). Staining for the pan-neuronal markers NeuN and Neuro-Chrom is shown in
550 yellow; scale bar = 20 µm.

551

552 expressing cells are present throughout the IC, but tdTomato expressing cells are present only
553 at the AAV injection site.

554 In every case that exhibited tdTomato expressing cells in the IC, clearly labeled axons
555 with terminal and en passant boutons could be seen in four areas: locally within the ipsilateral
556 IC (Figure 6B), in the contralateral IC (Figure 6C; this is consistent with the labeling of
557 commissural axons with hrGFP in Figure 1), in the ipsilateral nucleus of the brachium of the IC
558 (NBIC; Figure 6D), and in the ipsilateral medial geniculate nucleus (MG; Figure 6E). Fields of
559 axons and terminals in the IC and the MG were spread widely, without any apparent preference
560 for a specific subdivision. Less frequently, fewer axons with boutons were observed in other
561 targets, for example the contralateral NBIC and MG, the ipsilateral cuneiform nucleus, the
562 ipsilateral superior olivary complex, and the periaqueductal gray. These targets are largely
563 consistent with previous reports of projections of GABAergic IC cells.

564

565 **NPY hyperpolarizes a subset of Y_1R-expressing neurons in the IC**

566 Previous studies suggest that Y_1Rs are expressed in the IC (Kishi et al., 2005; Eva et al.,
567 2006), but it is not known whether NPY signaling affects the IC. To test whether NPY signaling
568 influences the excitability of IC neurons, we used Npy1r^{cre} x Ai14 mice to label Y_1R-expressing
569 neurons with the fluorescent protein tdTomato (Padilla et al., 2016). We found that Y_1R
570 neurons are broadly distributed in the IC (Figure 7A). Interestingly, we also observed that blood
571 vessels in the IC were lined with non-neuronal cells expressing Y_1R (Figure 7A green arrows).
572 Because NPY induces vasoconstriction in other brain regions (Bao et al., 1997; Cauli et al.,
573 2004), NPY signaling might regulate blood flow in the IC, an important hypothesis we will
574 pursue in a future study.

575 To test how activation of Y_1Rs affects excitability, we targeted current clamp recordings
576 to Y_1R neurons while including 1 µM tetrodotoxin in the bath to block endogenous release of
577 NPY from spontaneously active NPY neurons. We found that bath application of [Leu^{31}, Pro^{34}]-
578 NPY, a high-affinity Y_1R agonist, hyperpolarized V_{rest} in 50% of Y_1R neurons by an average of -6.2
579 ± 4.3 mV (n = 5 out of 10 neurons; two-tailed paired t-test comparing baseline V_{rest} to treatment

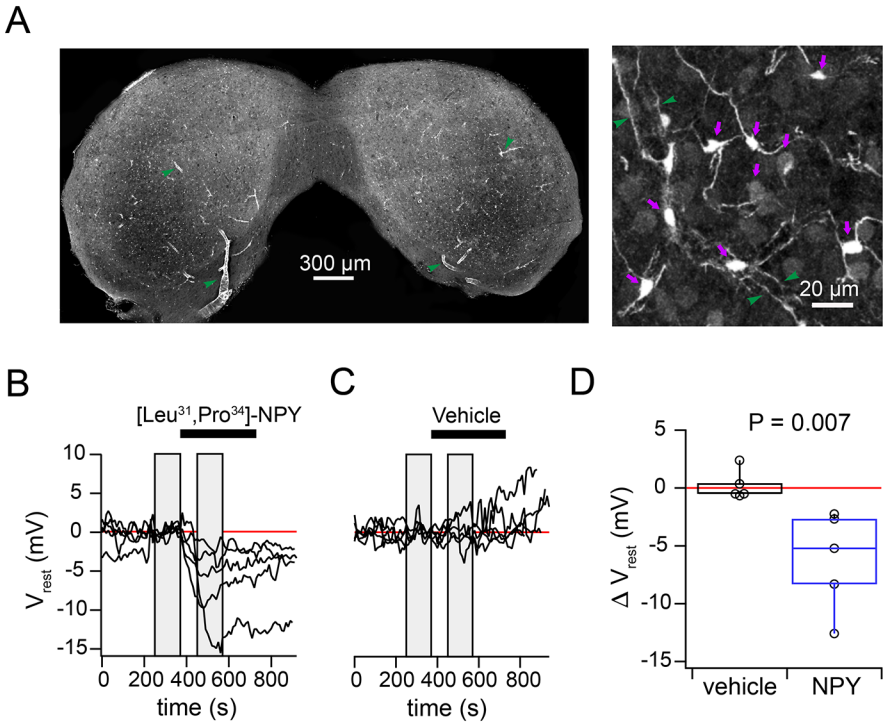

580

581 **Figure 7. [Leu^{31}, Pro^{34}]-NPY hyperpolarized V_{rest} in a subset of Y_1R-expressing IC neurons. *A,*** Left, tile scan
582 image showing the distribution of tdTomato expression in the IC of an Npy1r^{cre} x Ai14 mouse. Right, higher
583 magnification image. Magenta arrowheads indicate cell bodies of neurons that are tdTomato$^+$, indicating
584 that they express Y_1R. Green arrows indicate blood vessels lined with tdTomato$^+$ cells, reflecting the
585 likelihood that IC blood vessels also respond to NPY. ***B, C,*** Graphs showing 15 min of recording from
586 tdTomato$^+$ Y_1R neurons. Gray bars indicate periods in which baseline (left bar) and treatment (right bar)
587 measurements were made. ***B,*** Application of 500 nM [Leu^{31}, Pro^{34}]-NPY led to a hyperpolarizing shift in
588 the V_{rest} of 50% of tdTomato$^+$ neurons (-6.2 ± 4.3 mV change; n = 5 out of 10 neurons; two-tailed paired t-
589 test comparing baseline V_{rest} to treatment V_{rest}, p = 0.032). ***C,*** Vehicle had no effect on the membrane
590 potential of tdTomato$^+$ neurons (0.2 ± 1.3 mV change; n = 5; two-tailed paired t-test, p = 0.694). ***D,*** Boxplot
591 showing the change in V_{rest} between vehicle- and [Leu^{31}, Pro^{34}]-NPY-treated neurons (two-tailed Mann-
592 Whitney-Wilcoxon test, p = 0.007). Boxplots show median, 25th and 75th percentile (box), and 9th and 91st
593 percentile (whiskers).

594

595 V_{rest}, p = 0.032; Figure 7B). A neuron was considered sensitive to [Leu^{31}, Pro^{34}]-NPY when V_{rest}
596 hyperpolarized more than 2 mV below baseline in the presence of the drug. Neurons that did
597 not respond to the drug exhibited a -0.5 ± 0.8 mV change in V_{rest}, which was not significantly
598 different from the baseline V_{rest} (n= 5 out of 10 neurons; two-tailed paired t-test, p = 0.248). In
599 control experiments performed with a vehicle solution, there was no significant change in V_{rest}
600 between the baseline and vehicle periods (n = 5, 0.2 ± 1.3 mV; two-tailed paired t-test, p =
601 0.694; Figure 7C). Neurons that responded to [Leu^{31}, Pro^{34}]-NPY exhibited a significantly

602 different change in V_{rest} compared to neurons treated with vehicle (two-tailed Mann-Whitney-
603 Wilcoxon test, p = 0.007; Figure 7D). After a 30 – 50 minute wash-out period, the V_{rest} of all cells
604 that responded to [Leu^{31}, Pro^{34}]-NPY returned to baseline (n = 5, two-tailed paired t-test, p =
605 0.333; data not shown). Together, these results show that NPY signaling provides a novel
606 mechanism to dampen excitability in the IC. Since NPY neurons express NPY (Figure 2 A-C) and
607 provide bouton-laden axons to the local and contralateral IC (Figure 6), it is likely that at least
608 some NPY signaling in the IC originates from local NPY neurons.

609

610 **Discussion**

611 Using a multifaceted approach, we have identified NPY neurons as a novel class of
612 inhibitory principal neurons in the IC. NPY neurons are GABAergic, produce NPY, are present in
613 the three main subdivisions of the IC, and have a stellate morphology, with dendrites that cross
614 the isofrequency laminae of the ICc. Based on stereological analysis, we conclude that NPY
615 neurons account for approximately one-third of GABAergic neurons in the IC and 38 – 50% of
616 stellate neurons in the ICc. NPY neurons exhibited pacemaker activity, suggesting they might
617 tonically release GABA and NPY onto their postsynaptic targets. Viral tract tracing showed that
618 NPY neurons project to several targets, including the ipsilateral MG. We tested the effects of
619 NPY signaling in the IC and found the first evidence that NPY signaling can regulate the
620 membrane excitability of IC neurons. Thus, NPY neurons represent a major new class of IC
621 inhibitory neurons that may use both GABAergic and NPY signaling to regulate the activity of
622 neural circuits in the IC, NBIC and MG.

623

624 **NPY neurons are a distinct class of IC neurons**

625 The identification of fundamental neuron classes is essential for understanding the
626 organization and function of neural circuits in the brain. Previous studies showed that the IC
627 contains a large and diverse population of GABAergic neurons. These efforts relied on neuronal
628 morphology (Oliver et al., 1994), in vivo physiology (Ono et al., 2017), neurochemical and

629 extracellular markers (Ito et al., 2009; Beebe et al., 2016) or a combination of morphology,
630 physiology and neurotransmitter content (Ono et al., 2005). However, these studies yielded
631 different results, and it is unclear whether the types of GABAergic neurons they defined
632 represent functionally meaningful groups. In addition, because the neuron groups identified in
633 these studies lack molecular markers, they are not readily accessible for targeted manipulations
634 with optogenetics and other molecular tools.

635 In recent years, it has become clear that combining molecular markers with
636 physiological and anatomical parameters is key to identifying functionally relevant classes of
637 neurons (Tremblay et al., 2016; Zeng and Sanes, 2017). Through such an approach, we
638 identified NPY neurons as a distinct subtype of GABAergic stellate neurons. NPY neurons are
639 selectively labeled in NPY-hrGFP mice, and they share a common neurotransmitter content,
640 neuropeptide expression, stellate morphology, and similar physiological features. Ninety-nine
641 percent of NPY neurons immunostained for GAD67, and 95% immunostained for NPY. Ninety-
642 two percent of ICc NPY neurons met the criteria for stellate morphology. In our recordings, 90 –
643 92% of NPY neurons had a sustained firing pattern. Previously, Ono and colleagues reported
644 that GAD67^{+} neurons exhibited four firing patterns: regular sustained, buildup/pauser, and
645 transient with or without after-depolarizations (Ono et al., 2005). Our results show that NPY
646 neurons fit into the regular sustained category, which included 43% of GAD67^{+} neurons in the
647 Ono study.

648 We observed that most NPY neurons spontaneously fired at rest. Interestingly,
649 spontaneous firing has also been reported for NPY neurons in hypothalamus (Top et al., 2004),
650 striatum (Partridge et al., 2009) and amygdala (Song et al., 2016). This suggests that NPY
651 neurons in multiple brain regions might preferentially express a common suite of ion channels
652 that promotes spontaneous firing. The spontaneous firing of NPY neurons in the IC indicates
653 that NPY neurons in vivo might provide a constant tone of GABA and NPY to the IC, NBIC, and
654 MG. This inhibitory tone might be rapidly upregulated or downregulated by inputs that
655 modulate that activity levels of NPY neurons, providing a mechanism for NPY neurons to
656 increase or decrease the overall excitability in postsynaptic brain regions.

657

658 **NPY neurons are GABAergic projection neurons**

659 We found that NPY neurons project to several targets including the contralateral IC, the
660 ipsilateral NBIC and the ipsilateral MG. In most brain regions, GABAergic neurons are
661 interneurons (Tremblay et al., 2016), but the IC contains a large number of GABAergic neurons
662 that project to MG and other targets including NBIC and superior colliculus (Winer et al., 1996;
663 Peruzzi et al., 1997; Ito et al., 2009; Mellott et al., 2014, 2018; Beebe et al., 2018). The
664 functional roles of these inhibitory projections are largely unknown. The inhibitory projection to
665 MG is particularly interesting because other regions of primary sensory thalamus do not receive
666 ascending inhibitory input (Halassa and Acsády, 2016). Since NPY neurons are molecularly
667 identifiable, it is now possible to use optogenetics and other targeted approaches to test how a
668 specific inhibitory projection from the IC shapes activity in the MG and NBIC.

669

670 **NPY neurons likely use both GABA and NPY signaling to regulate activity in the IC and MG**

671 NPY is widely expressed in the central nervous system of mammals and is a potent
672 modulator of neuronal activity. Previous brain-wide screening studies suggested that NPY and
673 Y_1Rs are expressed in the IC (Widdowson, 1993; Kishi et al., 2005; Eva et al., 2006), but the
674 experiments conducted here are the first to characterize IC neurons that synthesize NPY and to
675 test the effects of NPY signaling on IC neurons. Y_1Rs tend to inhibit neurons when activated
676 (Giesbrecht et al., 2010). Consistent with this, we found that application of [Leu^{31}, Pro^{34}]-NPY
677 hyperpolarized V_{rest} in 50% of the tested Y_1R-expressing neurons. It has been shown that Y_1R
678 activation can induce opening of G protein-coupled inwardly rectifying potassium (G_{IRK})
679 channels, suggesting that G_{IRK} activation might mediate the effects we observed in the IC (Sun
680 et al., 2001; Paredes et al., 2003; Fu et al., 2004; Sosulina et al., 2008), although other
681 mechanisms are possible (Giesbrecht et al., 2010; Villarroel et al., 2018). The fact that not all IC
682 Y_1R neurons were sensitive to NPY might be due to transient developmental expression of Cre
683 in some neurons. Alternatively, non-responsive neurons might respond to NPY in ways that we
684 did not test.

685 It is likely that IC NPY neurons also use NPY signaling to influence targets beyond the IC.
686 Y_1R expression has been reported in the MG (Kishi et al., 2005), and we observed tdTomato
687 expression in a population of MG neurons in Npy1r^{cre} x Ai14 mice (data not shown). It is not yet
688 clear whether NPY receptors are expressed in the NBIC.

689 Beyond influencing auditory computations, the inhibitory effects of NPY signaling might
690 serve diverse roles in the IC. In the hippocampus and amygdala, NPY released from GABAergic
691 NPY neurons acts as an endogenous anticonvulsant (Colmers and Bleakman, 1994; Colmers and
692 El Bahh, 2003; Noe' et al., 2007). Interestingly, the IC is the main site of initiation of audiogenic
693 seizures (Ross and Coleman, 2000; Faingold, 2002), and therefore NPY neurons might use NPY
694 and GABA release to protect against hyperexcitability in the IC. Consistent with this, acoustic
695 trauma leads to an increase in the expression of brain-derived neurotrophic factor (BDNF) in
696 the IC (Meltser and Canlon, 2010), and, in other brain regions, it is known that BDNF can
697 enhance NPY expression (Nawa et al., 1994; Nobuyuki Takei et al., 1996; Wirth et al., 2005).

698 It has also been shown that the IC plays an important role in auditory task-related
699 unconditioned fear responses (Muthuraju et al., 2014; Oliveira et al., 2014) and anxiety (Silveira
700 et al., 1993). In the amygdala (Sajdyk et al., 2008), cortex (Vollmer et al., 2016) and
701 hippocampus (Li et al., 2017), NPY exhibits anti-anxiolytic properties and regulates behaviors
702 associated with fear. Thus, NPY neurons in the IC might regulate how IC circuits process
703 unconditioned fear responses and how they are affected by behavioral states like anxiety.

704 Interestingly, in the IC of Npy1r^{cre} x Ai14 mice we found strong labeling of cells
705 associated with blood vessels (Figure 7A). Previous studies showed that NPY induces
706 contraction in cortical microvessels by activating Y_1Rs (Abounader et al., 1999; Cauli et al.,
707 2004) and plays a similar role in the cochlea (Carlisle et al., 1990). Since the IC is reported to be
708 the most metabolically active brain region and to have the highest rate of blood flow in the
709 brain (Sokoloff et al., 1977; Gross et al., 1987; Zeller et al., 1997), IC NPY neurons might play a
710 critical role regulating energy homeostasis in the IC.

711

712 **NPY and VIP neurons account for more than half of ICc stellate neurons**

713 ICc stellate neurons have long been a subject of speculation, but their functional roles are almost
714 completely unknown due to lack of an approach to target or selectively manipulate them during
715 in vivo recordings or behavioral testing. We showed here that it is possible to selectively express
716 exogenous proteins in IC NPY neurons (Figure 6). In addition, we recently identified VIP neurons
717 as a novel class of glutamatergic stellate cells in the IC, and VIP neurons can be selectively
718 manipulated in VIP-IRES-Cre mice (Goyer et al., 2019). VIP and NPY neurons represent 3.5% and
719 7.6% of neurons in the ICc, respectively, and combined they account for approximately 55 – 74%
720 of ICc stellate neurons. Thus, for the first time, we are positioned to determine the functional
721 roles of excitatory and inhibitory stellate neurons that together represent the majority of ICc
722 stellate neurons.

723

724 **Conflict of Interest Statement:** The authors declare no competing financial interests.

725

726 **Acknowledgements:** We thank Bo Duan for helpful discussions and advice. This work was
727 supported by a Research Grant from the American Hearing Research Foundation (MAS) and
728 National Institutes of Health Grants R56 DC016880 (MTR) and R01 DC004391 (BRS).

729

730 **References**

731 Abounader R, Elhusseiny A, Cohen Z, Olivier A, Stanimirovic D, Quirion R, Hamel E (1999) Expression of
732 Neuropeptide Y Receptors mRNA and Protein in Human Brain Vessels and Cerebromicrovascular
733 Cells in Culture. J Cereb Blood Flow Metab 19:155–163.

734 Adams JC (1979) Ascending projections to the inferior colliculus. J Comp Neurol 183:519–538.

735 Bacci A, Huguenard JR, Prince DA (2002) Differential modulation of synaptic transmission by
736 neuropeptide Y in rat neocortical neurons. PNAS 99:17125–17130.

737 Bao L, Kopp J, Zhang X, Xu Z-QD, Zhang L-F, Wong H, Walsh J, Hökfelt T (1997) Localization of
738 neuropeptide Y Y1 receptors in cerebral blood vessels. PNAS 94:12661–12666.

739 Beebe NL, Mellott JG, Schofield BR (2018) Inhibitory Projections from the Inferior Colliculus to the
740 Medial Geniculate body Originate from Four Subtypes of GABAergic Cells. eNeuro
741 5:ENEURO.0406-18.2018.

742 Beebe NL, Young JW, Mellott JG, Schofield BR (2016) Extracellular Molecular Markers and Soma Size of
743 Inhibitory Neurons: Evidence for Four Subtypes of GABAergic Cells in the Inferior Colliculus. The
744 Journal of Neuroscience 36:3988–3999.

745 Buentello DC, Bishop DC, Oliver DL (2015) Differential Distribution of GABA and Glycine Terminals in
746 Inferior Colliculus of Rat and Mouse. J Comp Neurol 523:2683–2697.

747 Cant NB, Benson CG (2006) Organization of the inferior colliculus of the gerbil (Meriones unguiculatus):
748 differences in distribution of projections from the cochlear nuclei and the superior olivary
749 complex. J Comp Neurol 495:511–528.

750 Cant NB, Benson CG (2007) Multiple topographically organized projections connect the central nucleus
751 of the inferior colliculus to the ventral division of the medial geniculate nucleus in the gerbil,
752 Meriones unguiculatus. J Comp Neurol 503:432–453.

753 Carlisle L, Aberdeen J, Forge A, Burnstock G (1990) Neural basis for regulation of cochlear blood flow:
754 Peptidergic and adrenergic innervation of the spiral modiolar artery of the guinea pig. Hearing
755 Research 43:107–113.

756 Cauli B, Tong X-K, Rancillac A, Serluca N, Lambolez B, Rossier J, Hamel E (2004) Cortical GABA
757 interneurons in neurovascular coupling: relays for subcortical vasoactive pathways. J Neurosci
758 24:8940–8949.

759 Chambers AR, Resnik J, Yuan Y, Whitton JP, Edge AS, Liberman MC, Polley DB (2016) Central Gain
760 Restores Auditory Processing following Near-Complete Cochlear Denervation. Neuron 89:867–
761 879.

762 Chronwall BM, DiMaggio DA, Massari VJ, Pickel VM, Ruggiero DA, O'donohue TL (1985) The anatomy of
763 neuropeptide-y-containing neurons in rat brain. Neuroscience 15:1159–1181.

764 Colmers WF, Bleakman D (1994) Effects of neuropeptide Y on the electrical properties of neurons.
765 Trends in Neurosciences 17:373–379.

766 Colmers WF, El Bahh B (2003) Neuropeptide Y and Epilepsy. Epilepsy Curr 3:53–58.

767 Coote EJ, Rees A (2008) The distribution of nitric oxide synthase in the inferior colliculus of guinea pig.
768 Neuroscience 154:218–225.

769 Dumont Y, Jacques D, Bouchard P, Quirion R (1998) Species differences in the expression and
770 distribution of the neuropeptide Y Y1, Y2, Y4, and Y5 receptors in rodents, guinea pig, and
771 primates brains. Journal of Comparative Neurology 402:372–384.

772 Eva C, Serra M, Mele P, Panzica G, Oberto A (2006) Physiology and gene regulation of the brain NPY Y1
773 receptor. Frontiers in Neuroendocrinology 27:308–339.

774 Faingold CL (2002) Role of GABA abnormalities in the inferior colliculus pathophysiology - audiogenic
775 seizures. Hear Res 168:223–237.

776 Faye-Lund H, Osen KK (1985) Anatomy of the inferior colliculus in rat. Anat Embryol 171:1–20.

Foster NL, Mellott JG, Schofield BR (2014) Perineuronal nets and GABAergic cells in the inferior colliculus of guinea pigs. Front Neuroanat 7:53.

Fu L-Y, Acuna-Goycolea C, Pol AN van den (2004) Neuropeptide Y Inhibits Hypocretin/Orexin Neurons by Multiple Presynaptic and Postsynaptic Mechanisms: Tonic Depression of the Hypothalamic Arousal System. J Neurosci 24:8741–8751.

Giesbrecht CJ, Mackay JP, Silveira HB, Urban JH, Colmers WF (2010) Countervailing modulation of Ih by neuropeptide Y and corticotrophin-releasing factor in basolateral amygdala as a possible mechanism for their effects on stress-related behaviors. J Neurosci 30:16970–16982.

Goyer D, Silveira MA, George AP, Beebe NL, Edelbrock RM, Malinski PT, Schofield BR, Roberts MT (2019) A novel class of inferior colliculus principal neurons labeled in vasoactive intestinal peptide-Cre mice King AJ, Lee C, Oliver D, Borst JGG, eds. eLife 8:e43770.

Gross PM, Sposito NM, Pettersen SE, Panton DG, Fenstermacher JD (1987) Topography of Capillary Density, Glucose Metabolism, and Microvascular Function within the Rat Inferior Colliculus. J Cereb Blood Flow Metab 7:154–160.

Halassa MM, Acsády L (2016) Thalamic Inhibition: Diverse Sources, Diverse Scales. Trends in Neurosciences 39:680–693.

Henry FE, Sugino K, Tozer A, Branco T, Sternson SM (2015) Cell type-specific transcriptomics of hypothalamic energy-sensing neuron responses to weight-loss Elmquist JK, ed. eLife 4:e09800.

Ito T, Bishop DC, Oliver DL (2009) Two Classes of GABAergic Neurons in the Inferior Colliculus. Journal of Neuroscience 29:13860–13869.

Karagiannis A, Gallopin T, Dávid C, Battaglia D, Geoffroy H, Rossier J, Hillman EMC, Staiger JF, Cauli B (2009) Classification of NPY-Expressing Neocortical Interneurons. J Neurosci 29:3642–3659.

Keesom SM, Morningstar MD, Sandlain R, Wise BM, Hurley LM (2018) Social isolation reduces serotonergic fiber density in the inferior colliculus of female, but not male, mice. Brain Research 1694:94–103.

Kishi T, Aschkenasi CJ, Choi BJ, Lopez ME, Lee CE, Liu H, Hollenberg AN, Friedman JM, Elmquist JK (2005) Neuropeptide Y Y1 receptor mRNA in rodent brain: Distribution and colocalization with melanocortin-4 receptor. Journal of Comparative Neurology 482:217–243.

Ledoux VA, Smejkalova T, May RM, Cooke BM, Woolley CS (2009) Estradiol facilitates the release of NPY to suppress hippocampus-dependent seizures. J Neurosci 29:1457–1468.

Li Q, Bartley AF, Dobrunz LE (2017) Endogenously Released Neuropeptide Y Suppresses Hippocampal Short-Term Facilitation and Is Impaired by Stress-Induced Anxiety. J Neurosci 37:23–37.

Malmierca MS, Blackstad TW, Osen KK, Karagülle T, Molowny RL (1993) The central nucleus of the inferior colliculus in rat: a Golgi and computer reconstruction study of neuronal and laminar structure. J Comp Neurol 333:1–27.

812 Marshall CJ, Desroziers E, McLennan T, Campbell RE (2017) Defining Subpopulations of Arcuate Nucleus
813 GABA Neurons in Male, Female, and Prenatally Androgenized Female Mice. Neuroendocrinology
814 105:157–169.

815 Meininger V, Pol D, Derer P (1986) The inferior colliculus of the mouse. A Nissl and Golgi study.
816 Neuroscience 17:1159–1179.

817 Mellott JG, Beebe NL, Schofield BR (2018) GABAergic and non-GABAergic projections to the superior
818 colliculus from the auditory brainstem. Brain Structure and Function 223:1923–1936.

819 Mellott JG, Foster NL, Nakamoto KT, Motts SD, Schofield BR (2014) Distribution of GABAergic cells in the
820 inferior colliculus that project to the thalamus. Front Neuroanat 7:53.

821 Meltser I, Canlon B (2010) The expression of mitogen-activated protein kinases and brain-derived
822 neurotrophic factor in inferior colliculi after acoustic trauma. Neurobiology of Disease 40:325–
823 330.

824 Merchán M, Aguilar LA, Lopez-Poveda EA, Malmierca MS (2005) The inferior colliculus of the rat:
825 quantitative immunocytochemical study of GABA and glycine. Neuroscience 136:907–925.

826 Milner TA, Wiley RG, Kurucz OS, Prince SR, Pierce JP (1997) Selective changes in hippocampal
827 neuropeptide Y neurons following removal of the cholinergic septal inputs. Journal of
828 Comparative Neurology 386:46–59.

829 Milstein AD, Bloss EB, Apostolides PF, Vaidya SP, Dilly GA, Zemelman BV, Magee JC (2015) Inhibitory
830 Gating of Input Comparison in the CA1 Microcircuit. Neuron 87:1274–1289.

831 Morest DK, Oliver DL (1984) The neuronal architecture of the inferior colliculus in the cat: defining the
832 functional anatomy of the auditory midbrain. J Comp Neurol 222:209–236.

833 Muthuraju S, Nobre MJ, Saito VMN, Brandao ML (2014) Distinct effects of haloperidol in the mediation
834 of conditioned fear in the mesolimbic system and processing of unconditioned aversive
835 information in the inferior colliculus. Neuroscience 261:195–206.

836 Nakagawa H, Ikeda M, Houtani T, Ueyama T, Baba K, Kondoh A, Yamamoto T, Yamashita T, Sugimoto T
837 (1995) Immunohistochemical evidence for enkephalin and neuropeptide Y in rat inferior
838 colliculus neurons that provide ascending or commissural fibers. Brain Res 690:236–240.

839 Nawa H, Pelleymounter MA, Carnahan J (1994) Intraventricular administration of BDNF increases
840 neuropeptide expression in newborn rat brain. J Neurosci 14:3751–3765.

841 Noben-Trauth K, Zheng QY, Johnson KR (2003) Association of cadherin 23 with polygenic inheritance and
842 genetic modification of sensorineural hearing loss. Nat Genet 35:21–23.

843 Nobuyuki Takei, Kumi Sasaoka, Hiroshi Higuchi, Yasuhisa Endo, Hiroshi Hatanaka (1996) BDNF increases
844 the expression of neuropeptide Y mRNA and promotes differentiation/maturation of
845 neuropeptide Y-positive cultured cortical neurons from embryonic and postnatal rats. Molecular
846 Brain Research 37:283–289.

847 Noe' F, Nissinen J, Pitkänen A, Gobbi M, Sperk G, During M, Vezzani A (2007) Gene therapy in epilepsy:
848 The focus on NPY. Peptides 28:377–383.

849 O'Donohue TL, Chronwall BM, Pruss RM, Mezey E, Kiss JZ, Eiden LE, John Massari V, Tessel RE, Pickel
850 VM, DiMaggio DA, Hotchkiss AJ, Crowley WR, Zukowska-Grojec Z (1985) Neuropeptide Y and
851 peptide YY neuronal and endocrine systems. Peptides 6:755–768.

852 Oliveira AR de, Colombo AC, Muthuraju S, Almada RC, Brandão ML (2014) Dopamine D2-Like Receptors
853 Modulate Unconditioned Fear: Role of the Inferior Colliculus. PLOS ONE 9:e104228.

854 Oliver DL, Kuwada S, Yin TC, Haberly LB, Henkel CK (1991) Dendritic and axonal morphology of HRP-
855 injected neurons in the inferior colliculus of the cat. J Comp Neurol 303:75–100.

856 Oliver DL, Morest DK (1984) The central nucleus of the inferior colliculus in the cat. Journal of
857 Comparative Neurology 222:237–264.

858 Oliver DL, Winer JA, Beckius GE, Saint Marie RL (1994) Morphology of GABAergic neurons in the inferior
859 colliculus of the cat. J Comp Neurol 340:27–42.

860 Ono M, Bishop DC, Oliver DL (2017) Identified GABAergic and Glutamatergic Neurons in the Mouse
861 Inferior Colliculus Share Similar Response Properties. J Neurosci 37:8952–8964.

862 Ono M, Yanagawa Y, Koyano K (2005) GABAergic neurons in inferior colliculus of the GAD67-GFP knock-
863 in mouse: Electrophysiological and morphological properties. Neuroscience Research 51:475–
864 492.

865 Padilla SL, Qiu J, Soden ME, Sanz E, Nestor CC, Barker FD, Quintana A, Zweifel LS, Rønnekleiv OK, Kelly
866 MJ, Palmiter RD (2016) Agouti-related peptide neural circuits mediate adaptive behaviors in the
867 starved state. Nature Neuroscience 19:734–741.

868 Palmer AR, Shackleton TM, Sumner CJ, Zobay O, Rees A (2013) Classification of frequency response
869 areas in the inferior colliculus reveals continua not discrete classes. J Physiol (Lond) 591:4003–
870 4025.

871 Paredes MF, Greenwood J, Baraban SC (2003) Neuropeptide Y modulates a G protein-coupled inwardly
872 rectifying potassium current in the mouse hippocampus. Neuroscience Letters 340:9–12.

873 Partridge JG, Janssen MJ, Chou DYT, Abe K, Zukowska Z, Vicini S (2009) Excitatory and Inhibitory
874 Synapses in Neuropeptide Y–Expressing Striatal Interneurons. Journal of Neurophysiology
875 102:3038–3045.

876 Peruzzi D, Bartlett E, Smith PH, Oliver DL (1997) A monosynaptic GABAergic input from the inferior
877 colliculus to the medial geniculate body in rat. J Neurosci 17:3766–3777.

878 Peruzzi D, Sivaramakrishnan S, Oliver DL (2000) Identification of cell types in brain slices of the inferior
879 colliculus. Neuroscience 101:403–416.

880 Polgár E, Sardella TC, Watanabe M, Todd AJ (2011) Quantitative Study of NPY-Expressing GABAergic
881 Neurons and Axons in Rat Spinal Dorsal Horn. J Comp Neurol 519:1007–1023.

882 Roa J, Herbison AE (2012) Direct Regulation of GnRH Neuron Excitability by Arcuate Nucleus POMC and
883 NPY Neuron Neuropeptides in Female Mice. Endocrinology 153:5587–5599.

884 Rose JB, Crews L, Rockenstein E, Adame A, Mante M, Hersh LB, Gage FH, Spencer B, Potkar R, Marr RA,
885 Masliah E (2009) Neuropeptide Y Fragments Derived from Neprilysin Processing Are
886 Neuroprotective in a Transgenic Model of Alzheimer's Disease. J Neurosci 29:1115–1125.

887 Ross KC, Coleman JR (2000) Developmental and genetic audiogenic seizure models: behavior and
888 biological substrates. Neuroscience & Biobehavioral Reviews 24:639–653.

889 Rowan S, Todd AJ, Spike RC (1993) Evidence that neuropeptide Y is present in gabaergic neurons in the
890 superficial dorsal horn of the rat spinal cord. Neuroscience 53:537–545.

891 Saint Marie RL, Stanforth DA, Jubelier EM (1997) Substrate for rapid feedforward inhibition of the
892 auditory forebrain. Brain Research 765:173–176.

893 Sajdyk TJ, Johnson PL, Leitermann RJ, Fitz SD, Dietrich A, Morin M, Gehlert DR, Urban JH, Shekhar A
894 (2008) Neuropeptide Y in the Amygdala Induces Long-Term Resilience to Stress-Induced
895 Reductions in Social Responses But Not Hypothalamic–Adrenal–Pituitary Axis Activity or
896 Hyperthermia. J Neurosci 28:893–903.

897 Silveira MCL, Sandner G, Graeff FG (1993) Induction of Fos immunoreactivity in the brain by exposure to
898 the elevated plus-maze. Behavioural Brain Research 56:115–118.

899 Sokoloff L, Reivich M, Kennedy C, Rosiers MHD, Patlak CS, Pettigrew KD, Sakurada O, Shinohara M (1977)
900 The [14c]deoxyglucose Method for the Measurement of Local Cerebral Glucose Utilization:
901 Theory, Procedure, and Normal Values in the Conscious and Anesthetized Albino Rat1. Journal
902 of Neurochemistry 28:897–916.

903 Song SC, Beatty JA, Wilson CJ (2016) The ionic mechanism of membrane potential oscillations and
904 membrane resonance in striatal LTS interneurons. Journal of Neurophysiology 116:1752–1764.

905 Sosulina L, Schwesig G, Seifert G, Pape H-C (2008) Neuropeptide Y activates a G-protein-coupled
906 inwardly rectifying potassium current and dampens excitability in the lateral amygdala. Mol Cell
907 Neurosci 39:491–498.

908 Stiebler I, Ehret G (1985) Inferior colliculus of the house mouse. I. A quantitative study of tonotopic
909 organization, frequency representation, and tone-threshold distribution. Journal of Comparative
910 Neurology 238:65–76.

911 Sturm JJ, Zhang-Hooks Y-X, Roos H, Nguyen T, Kandler K (2017) Noise Trauma-Induced Behavioral Gap
912 Detection Deficits Correlate with Reorganization of Excitatory and Inhibitory Local Circuits in the
913 Inferior Colliculus and Are Prevented by Acoustic Enrichment. J Neurosci 37:6314–6330.

914 Sun QQ, Huguenard JR, Prince DA (2001) Neuropeptide Y receptors differentially modulate G-protein-
915 activated inwardly rectifying K+ channels and high-voltage-activated Ca2+ channels in rat
916 thalamic neurons. J Physiol (Lond) 531:67–79.

917 Tang JCY, Rudolph S, Dhande OS, Abraira VE, Choi S, Lapan SW, Drew IR, Drokhlyansky E, Huberman AD,
918 Regehr WG, Cepko CL (2015) Cell type–specific manipulation with GFP-dependent Cre
919 recombinase. Nature Neuroscience 18:1334–1341.

920 Tong Q, Ye C-P, Jones JE, Elmquist JK, Lowell BB (2008) Synaptic release of GABA by AgRP neurons is
921 required for normal regulation of energy balance. Nature Neuroscience 11:998–1000.

922 Top M van den, Lee K, Whyment AD, Blanks AM, Spanswick D (2004) Orexigen-sensitive NPY/AgRP
923 pacemaker neurons in the hypothalamic arcuate nucleus. Nat Neurosci 7:493–494.

924 Tremblay R, Lee S, Rudy B (2016) GABAergic Interneurons in the Neocortex: From Cellular Properties to
925 Circuits. Neuron 91:260–292.

926 van den Pol AN, Yao Y, Fu L-Y, Foo K, Huang H, Coppari R, Lowell B, Broberger C (2009) Neuromedin B
927 and gastrin releasing peptide excite arcuate nucleus neuropeptide Y neurons in a novel
928 transgenic mouse expressing strong renilla GFP in NPY neurons. J Neurosci 29:4622–4639.

929 Villarroel HS, Bompolaki M, Mackay J, Tapia APM, Michaelson SD, Leitermann RJ, Marr RA, Urban JH,
930 Colmers WF (2018) NPY induces stress resilience via down-regulation of Ih in principal neurons
931 of rat basolateral amygdala. J Neurosci:3528–17.

932 Vollmer LL, Schmeltzer S, Schurdak J, Ahlbrand R, Rush J, Dolgas CM, Baccei ML, Sah R (2016)
933 Neuropeptide Y Impairs Retrieval of Extinguished Fear and Modulates Excitability of Neurons in
934 the Infralimbic Prefrontal Cortex. Journal of Neuroscience 36:1306–1315.

935 Wallace MN, Shackleton TM, Palmer AR (2012) Morphological and physiological characteristics of
936 laminar cells in the central nucleus of the inferior colliculus. Front Neural Circuits 6:55.

937 West MJ, Slomianka L, Gundersen HJG (1991) Unbiased stereological estimation of the total number of
938 neurons in the subdivisions of the rat hippocampus using the optical fractionator. The
939 Anatomical Record 231:482–497.

940 Widdowson PS (1993) Quantitative receptor autoradiography demonstrates a differential distribution of
941 neuropeptide-Y Y1 and Y2 receptor subtypes in human and rat brain. Brain Research 631:27–38.

942 Winer JA, Saint Marie RL, Larue DT, Oliver DL (1996) GABAergic feedforward projections from the
943 inferior colliculus to the medial geniculate body. Proceedings of the National Academy of
944 Sciences 93:8005–8010.

945 Wirth MJ, Patz S, Wahle P (2005) Transcellular induction of neuropeptide Y expression by NT4 and BDNF.
946 PNAS 102:3064–3069.

947 Zeller K, Rahner-Welsch S, Kuschinsky W (1997) Distribution of Glut1 Glucose Transporters in Different
948 Brain Structures Compared to Glucose Utilization and Capillary Density of Adult Rat Brains. J
949 Cereb Blood Flow Metab 17:204–209.

950 Zeng H, Sanes JR (2017) Neuronal cell-type classification: challenges, opportunities and the path
951 forward. Nature Reviews Neuroscience 18:530–546.

952

953 **Key Resources Table**

Animals			
Species	**Designation**	**Source**	**Identifiers**
Genetic reagent (*mus musculus*)	NPY-hrGFP	The Jackson Laboratory	JAX:006417
Genetic reagent (*mus musculus*)	Npy1r$^{cre:GFP}$	The Jackson Laboratory	JAX:030544
Genetic reagent (*mus musculus*)	Ai14	The Jackson Laboratory	JAX:007914
Antibodies			
Designation	**Source**	**Identifiers**	**Concentration**
anti-GAD67 (mouse monoclonal)	Millipore	Cat#: MAB5406 RRID: AB_2278725	IHC:1:1000
anti-NeuN (rabbit polyclonal)	Millipore	Cat#: ABN78 RRID:AB_10807945	IHC: 1:500
anti-NPY (rabbit polyclonal)	Peninsula Labs	Cat#: T-4070 RRID: AB_518504	IHC: 1:1000
anti-bNOS (mouse monoclonal)	Sigma-Aldrich	Cat#: N2280 RRID: AB_260754	IHC: 1:1000
anti-GlyT2 (Guinea pig polyclonal)	Synaptic Systems	Cat#: 272 004 RRID: AB_2619998	IHC: 1:2500
anti-rabbit IgG Alexa Fluor 647 (donkey polyclonal)	ThermoFisher	Cat#: A31573 RRID: AB_2536183	IHC: 1:500
anti-mouse IgG Alexa Fluor 647 (donkey polyclonal)	ThermoFisher	Cat#: A-31571 RRID: AB_162542	IHC: 1:500
anti-guinea pig IgG Alexa Fluor 594 (goat polyclonal)	ThermoFisher	Cat#: A-11076 RRID: AB_141930	IHC: 1:500
Chemical compunds/drugs			
Designation	**Source**	**Identifiers**	**Concentration**
D-AP5	Hello Bio	Cat#: HB0225	50 µM
NBQX	Hello Bio	Cat#: HB0443	10 µM
TTX	Hello Bio	Cat#: HB1035	1µM
[Leu31,Pro34] NPY	Tocris	Cat#: 1176	500 nM
Recombinant DNA reagent			
Designation	**Source**		**Identifiers**
rAAV2/1-EF1a-N-CretrcintG	Boston Children's Hospital Viral Core		Addgene # 69570
rAAV2/1-EF1a-C-CreintG	Boston Children's Hospital Viral Core		Addgene # 69571
AAV1.CAG.LSL.tdTomato	University of Pennsylvania Vector Core		Addgene # 100048
Software, algorithm			

Designation	Source	Identifiers
Igor Pro 7 and 8	Wavemetrics	RRID:SCR_000325
Neurolucida	MBF Bioscience	RRID:SCR_001775
Neurolucida 360	MBF Bioscience	RRID:SCR_016788